Core orientations and magnetic fields in isolated molecular clouds

Ekta Sharma, 1,2,3 * Maheswar Gopinathan, 1 Archana Soam, 1,4 Chang Won Lee^{5,6} and T. R. Seshadri⁷

- ¹Indian Institute of Astrophysics (IIA), Sarjapur Road, Kormangala, Bangalore 560034, India
- ²Physical Research Laboratory, Navrangpura, Ahmedabad 380009, India
- ³National Astronomical Observatories, Chinese Academy of Sciences, Beijing, China
- ⁴SOFIA Science Centre, USRA, NASA Ames Research Centre, MS-12, N232, Moffett Field, CA 94035, USA
- ⁵Korea Astronomy & Space Science Institute, 776 Daedeokdae-ro, Yuseong-gu, Daejeon, Republic of Korea
- ⁶ University of Science and Technology, Korea (UST), 217 Gajeong-ro, Yuseong-gu, Daejeon 34113, Republic of Korea

Accepted XXX. Received YYY; in original form ZZZ

ABSTRACT

Molecular clouds are sites of star formation. Magnetic fields are believed to play an important role in their dynamics and shaping morphology. We aim to study any possible correlation that might exist between the magnetic fields orientation inside the clouds and the magnetic fields at envelope scales and their connection with respect to the observed morphology of the selected clouds. We examine the magnetic field orientation towards the clouds L1512, L1523, L1333, L1521E, L1544, L1517, L1780 and L183 using optical and *Planck* polarization observations. We also found the correlation between the ambient magnetic field and core orientations derived using *Astrodendrogram* on the *Herschel* 250 μ m data. We find that the magnetic fields derived from optical and *Planck* agree with each other. The derived magnetic fields are aligned along the observed emission of each cloud as seen in *Herschel* 250 μ m data. We also find that the relative orientation between the cores and the magnetic fields is random. This lack of correlation may arise due to the fact that the core orientation could also be influenced by the different magnetization within individual clouds at higher densities or the feedback effects which may vary from cloud to cloud. The estimated magnetic field strength and the mass-to-flux ratio suggest that all the clouds are in a magnetically critical state except L1333, L1521E and L183 where the cloud envelope could be strongly supported by the magnetic field lines.

Key words: Techniques: polarimetric - Parallaxes, formation - ISM: clouds, magnetic field

1 INTRODUCTION

In molecular clouds, the filamentary structures are ubiquitous and some of them are believed to be created by compression of material due to multi-scale supersonic flows (Alves et al. 2014). Localised density enhancements will shrink under self-gravity to form prestellar cores where stars form through collapsing gas motions (Shu et al. 1987). These prestellar cores are the preferential and ideal sites of star formation in nearby dark clouds like the Taurus and the Perseus (Ward-Thompson et al. 1994; Hatchell et al. 2005). Previous studies based on the optical inspection of the Palomar sky plate and molecular line observations in NH₃ and N₂H⁺ showed that the dense cores are typically of size ~ 0.1 pc and contain a few solar mass of subsonic material at temperatures of ~ 10 K and with an average volume density $\sim 10^4$ cm⁻³ (Myers & Benson 1983; Benson & Myers 1983). The correlation of dense core positions with the locations of highly embedded young stellar objects (YSOs) led to an idea that some cores are forming stars currently or some of them have initiated such formation very recently. On the basis of association of YSO or IRAS point source, the cores are broadly divided into two categories: prestellar and protostellar. The morphology of their emission can be observed in dust continum and molecular line observations. The results from the *Herschel* Gould Belt survey suggest that the cores are mostly being embedded in the filaments (André et al. 2010; Klessen & Hennebelle 2010; Alves et al. 2014). The association is consistent with the theoretical prediction that the thermally supercritical filaments experience a longitudinal fragmentation into cores (Inutsuka & Miyama 1992).

The significance of magnetic fields in the star formation process has been a subject of debate (e.g., Crutcher 2012; Li et al. 2014). It is widely believed that the magnetic fields along with the other physical factors like turbulence and gravity are the key factors affecting the star formation process at different scales and different evolutionary stages (Ballesteros-Paredes et al. 2007; McKee & Ostriker 2007). The magnetic fields can regulate the gravitational contraction of the cloud at higher densities ($n \ge 10^3 \text{ cm}^{-3}$) thus providing evidence of the field lines being dynamically important (Li et al. 2011). Several studies have been carried out to understand the dynamical importance of magnetic fields (Alves et al. 2008; Sugitani et al. 2010; Commerçon et al. 2011; Palau et al. 2013; Neha et al. 2016; Soam et al. 2018; Sharma et al. 2020).

The cloud-scale magnetic field at the lower densities can affect the compression in turbulence-induced shocks and channel the flows towards the high density regions (Heyer et al. 2008; Chen & Ostriker 2015). The core-scale magnetic field regulates the gas dynamics within the cores by removing angular momentum in collapsing cores and flattening the cores through the mechanism of ambipolar

⁷Department of Physics and Astrophysics, University of Delhi, Delhi 110007, India

^{*} E-mail: ektasharma.astro@gmail.com

diffusion. The correlation between the magnetic fields in the dense cores and the core orientation has been studied in various starless and star-forming regions (Ward-Thompson et al. 2000; Kirk et al. 2006). The magnetic fields at the intermediate scales connecting the large scale magnetic field to the field within cores can have a significant effect on their dynamics and the structure. Using the Planck polarization observations, Li et al. (2017) suggested a bimodal distribution in the alignment between the elongation of cloud (direction of major axes) and the direction of magnetic field using the Planck observations indicating that the alignment is more likely either parallel or perpendicular. Their study found the magnetic field as a primary regulator of the star formation rate. When the overall cloud evolves as a consequence of internal dynamics and stellar feedback effects, the clumps will also grow by accreting material turning into a non-spherical structures (Chen & Ostriker 2014, 2018; Kudoh & Basu 2011). Hence, clump shapes and orientation might be an indicator of formation mechanism. As a result of the interaction between magnetic field and core material through well defined orientation, the collapse may get inhibited and will result in reducing the star formation rate (Basu & Mouschovias 1995; Nakamura & Li 2011; Bailey et al. 2017). Therefore, it is crucial to explore the effect of large-scale magnetic field orientation on the morphology of dense core structures.

Observational studies were conducted by Poidevin et al. (2014) on the cores extracted from 350 µm Herschel observations to investigate the core orientations in the Lupus I cloud with respect to the large-scale magnetic field. The environment plays an important role in shaping the prestellar cores through ram pressure and magnetic pressure (Chen & Ostriker 2018). Cores are usually either oblate or prolate shaped structures as suggested by MHD simulations (Chen & Ostriker 2018; Banerjee et al. 2009). There are anisotropic gas flows along the magnetic field lines during the formation and evolution of cores which lead to the preferential orientation of the cores along the background magnetic field lines (Chen & Ostriker 2014, 2015). Chen et al. (2020), by combining simulations and observational results from the archive, studied a sample of cores in three clouds and investigated whether there is any systematic relation between the core orientation and the cloud-scale magnetic field. They found that the correlation has a regional dependence on the individual magnetic properties of the clouds. Optical polarization of starlight is used as a technique to trace the plane-of-sky magnetic field geometry which typically works in regions of low extinction (A_V \sim 1-3) (Goodman et al. 1990). Thus, optical polarimetry is mainly applicable towards the low density parts of the clouds. This is because the non-spherical dust grains which are believed to be aligned with their major axes perpendicular to the magnetic field cause selective extinction making the starlight polarized. At higher extinctions, the background starlight gets extinguished completely making it impossible to measure any polarization (e.g., Hiltner 1949; Vrba et al. 1976; Goodman et al. 1990; Alves et al. 2008; Soam et al. 2013). The polarized thermal dust emission is used as a technique to trace the plane-of-sky magnetic field geometry of regions with high obscurations (Ward-Thompson et al. 2009). This is because the nonspherical dust grains that are believed to be aligned with their major axes perpendicular to the magnetic field emit the radiation which is polarized in a direction parallel to the major axis of the dust grains. The all-sky maps of polarized emission from dust using the Planck satellite at 353 GHz gives a useful insight into the Galactic magnetic field in the star-forming regions (Planck Collaboration et al. 2016).

In this paper, we present results of a study conducted on eight clouds that are found to manifest their physical appearance in the form of sharp edges on one side and an extended diffuse emis-

Table 1. Log of the observations.

ID	Cloud Id.	Date of observations
1	L1333	10 December 2015; 11,12 January 5,6 February 2016
2	L1521E	10, 16 January; 8 February 2013
3	L1517	28 November; 1, 28 December 2013
4	L1512	26-30 October, 2017
5	L1544	23-25 January, 2014
6	L1523	28 October; 23, 24, 25 November 2016

sion of material on the opposite side of the clouds. The possible reasons behind this morphological emission could be the isotropic interstellar radiation field (ISRF) or the heating effect from nearby stars which may have interacted with the cloud material during the process of their evolution (Nielbock et al. 2012; Nutter et al. 2009; Launhardt et al. 2013; Kim et al. 2016). In Fig. 1, we show the fields contained the clouds using the *Herschel* 250 μ m SPIRE images of L1512, L1521E, L1517, L1544, L1780 and L183. The fields containing L1523 and L1333 are shown using the *Dobashi* extinction maps since there is no *Herschel* data available for them. The naming convention for the clouds given here are used to represent the whole cloud as shown in Fig. 1. The white solid contours drawn on the images reveal the emission morphology of the clouds. Basic information of these eight clouds are given in columns 1-5 of Table 2.

The questions that we are trying to investigate are the following: What is the relationship between the magnetic field orientations inside the clouds inferred from the *Planck* polarization and the envelope-field inferred from the optical polarization measurements of background starlight? What is the relationship between the magnetic field orientation with respect to the elongated morphology of the whole cloud? How the core major axes are oriented with respect to both inside and outside magnetic field directions? This paper is organised in the following manner. We begin with the observations and the data reduction. Then, we present results from our R-band polarization measurements and describe the procedure adapted to extract the cores in each cloud. We discussed our main results for each cloud on magnetic field geometry, strength and conclude the results with a summary in last section.

2 OBSERVATIONS AND DATA REDUCTION

The polarization measurements of stars projected on L1512, L1523, L1333, L1521E, L1517 and L1544 were carried out using ARIES Imaging Polarimeter (AIMPOL; Rautela et al. 2004) which is mounted on 1.04 m Sampurnanand Telescope (ST) at Nainital, India. The polarization measurements were done in the standard Johnson R-band filter. The details on the polarization measurements of clouds L1780 and L183 are given in Neha et al. (2016). Table 1 shows the log of the observations for all six clouds. The AIMPOL has a combination of an achromatic half-wave plate (HWP) modulator and a Wollaston prism in form of a beam splitter. It splits the incoming light into two rays - ordinary (I_o) and extra-ordinary (I_e). The observations were made at $\lambda_{eff} = 0.63 \ \mu m$. The plate scale of the CCD is 1.48''/pixel and the field of view is $\sim 8'$ in diameter which covers 325×325 pixel² area on the CCD. The full width at half-maximum of the stellar image varies from 2.9" to 4.4" (2-3 pixels) due to seeing of the atmosphere. The read-out noise and gain of CCD are 7.0 e^{-1} and 11.98 e^{-1} /ADU, respectively.

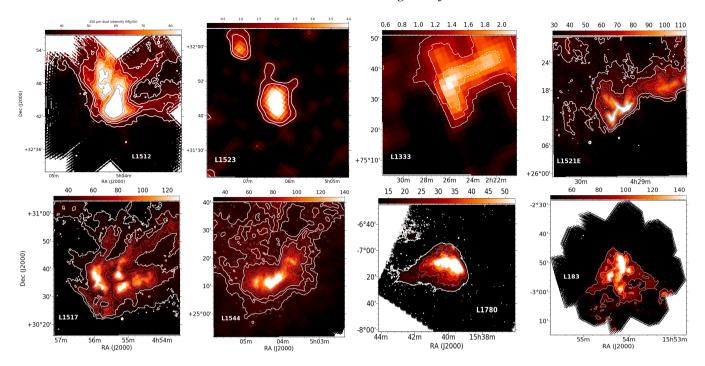


Figure 1. Left: The Herschel 250 μ m SPIRE image of size $0.5^{\circ} \times 0.5^{\circ}$ for L1512, L1521E, L1544, L1780 and L183 cloud and $0.8^{\circ} \times 0.8^{\circ}$ for L1517 with intensity contours shown in white lines. The Dobashi emission maps of size $0.5^{\circ} \times 0.5^{\circ}$ for L1523 and $0.75^{\circ} \times 0.75^{\circ}$ for L1333.

The standard aperture photometry available in the IRAF package was used to extract the fluxes of ordinary (I_o) and extraordinary (I_e) images of all the observed sources with a good signal-to-noise ratio. The ratio $R(\alpha)$ is given by,

$$R(\alpha) = \frac{\frac{I_{\epsilon}(\alpha)}{I_{\delta}(\alpha)} - 1}{\frac{I_{\epsilon}(\alpha)}{I_{\epsilon}(\alpha)} + 1} = P\cos(2\theta - 4\alpha),\tag{1}$$

where P (%) is the fraction of the total linearly polarized light, θ is the polarization angle in the plane-of-sky and the α is the position angle of the fast axis of the half-wave plate with respect to the axis of the Wollaston prism. The P and θ are calculated using the combination of the normalized stokes parameters q1, u1 and q2, u2 at angles 0° , 22.5° , 45° , 67.5° , respectively.

Instrumental polarization was evaluated by observing zeropolarization standard stars during every observation run. The typical instrumental polarization is found to be of the order of $\sim 0.1\%$ (Soam et al. 2013, 2015; Neha et al. 2016). The reference direction of the polarizer was determined by observing polarized standard stars taken from Schmidt et al. (1992). The zero point correction in the polarization angle was derived using the offset obtained between the position value obtained in our observations and the standard position angles given in Schmidt et al. (1992).

3 THE DATA FROM ARCHIVE

3.1 The Planck polarization

We used the 353 GHz (850 μ m) all-sky map of the polarized emission from dust provided by *Planck* Legacy Archive¹. The 353 GHz

channel in *Planck* satellite is the highest-frequency polarization-sensitive channel. We constructed the geometry of the magnetic fields for the whole sample based on the *Planck* polarization maps. The gnomonic projection of HEALPix software (Zonca et al. 2019; Górski et al. 2005) has been used to construct the stokes Q, U and I maps using all-sky *Planck* data. Then, the stokes maps were smoothed down to the 8' resolution to obtain a good signal-to-noise (SNR) ratio. We estimated linearly polarized intensity which is the quadrature sum of Stokes Q and U:

$$P = \sqrt{Q^2 + U^2},\tag{2}$$

The dust emission is linearly polarized with the electric vector normal to the sky-projected magnetic field. Therefore, the polarization position angles were rotated by 90° to infer the projected magnetic field as follows:

$$B_{pos} = \frac{1}{2}\arctan(-U,Q) + \pi/2. \tag{3}$$

The positions angles have been taken in accordance with HEALPix standards (Planck Collaboration et al. 2015) and converted to IAU convention by multiplying stokes U with -1 as shown in above equation. The zero position angle is oriented along the Galactic North and increases towards East of North on the sky.

3.2 The GAIA EDR3 data

We have used *Gaia* early data release 3 (EDR3) (Gaia Collaboration et al. 2021) for the distance measurements of the stars used in the polarimetric observations. The *Gaia* EDR3 data contains precise and updated astrometric as well as photometric parameters of ~ 2 billion stars. The survey lists the magnitude values at the broadband photometric bands of G, G_{BP} and G_{RP} in the wavelength range of 330-1050 nm (Gaia Collaboration et al. 2021). The distances to the stars studied in this work are obtained from the catalogue provided

¹ http://www.cosmos.esa.int/web/planck/pla/

by Bailer-Jones et al. (2021). The limiting magnitude of the sources for the distance calculation is ~ 21 in G-band. The uncertainties in the obtained parallax values vary from 0.02-0.03 milliarcsecond (mas) to 0.07 mas for sources with G < 15 mag and G = 17 mag, respectively. The uncertainties in the parallax values are ~ 0.5 mas for the fainter sources with G \sim 20 mag (Lindegren et al. 2021).

4 RESULTS

The degree of polarization (Pop%) and the polarization position angle (θ_{op} in degrees) of the stars projected on the molecular clouds from R-band observations are presented in Fig. 2. We plotted in the figure the data only for which the ratio of the Pop % and the error in the degree of polarization (e_n) greater than 3. The number of stars thus finally observed towards each cloud are listed in column 6 of Table 2. The mean value of $P_{op}\%$ and the standard deviation obtained from the stars projected on each cloud are given in column 7 of Table 2. In lower panels of Fig. 2 for each cloud, we also show the histogram of the θ_{op} . Based on a Gaussian fit to the data, the mean values of the θ_{op} for the stars projected on each cloud are obtained and listed in column 8 of Table 2. The polarization results obtained from the *Planck* data for all the eight clouds are also shown in Fig. 2. The Planck polarization results are selected from the regions where the 250 μ m intensity is greater than the standard deviation above the background intensity by a factor of three. The mean values of the polarization position angles (θ_{nlk}) and corresponding standard deviations are given in column 9 of Table 2.

4.1 The magnetic field geometry and the cloud morphology

The magnetic field geometry of a cloud is traced using the polarisation measurements of the stars that are background to the cloud. With the Gaia EDR3 data, we can ascertain whether the projected stars for which we have polarization measurements are foreground or background to the molecular clouds. If the observed star is background, the starlight will pass through the cloud and the asymmetric dust grains present in the clouds that are aligned with their minor axis parallel to the ambient magnetic field interact with the starlight. The starlight becomes polarized due to selective extinction and the polarization position angle gives the orientation of the projected magnetic field which is a projected component of the magnetic field in the plane of the sky (Davis & Greenstein 1951; Lazarian 2007). We obtained the distances of the stars having R-band polarization measurements from the Bailer-Jones et al. (2021) catalogue by making a search around each star with a search radius of 1". For the majority of the stars, we obtained a GAIA EDR3 counterpart well within our search radius. The Pop % vs. distance plot for the stars observed by us are presented in Fig. 3. For all the eight clouds, almost all the observed stars are found to lie beyond the distances quoted in column 4 of Table 2. This implies that the θ_{op} obtained from the R-band polarization measurements are tracing the projected component of the magnetic fields of the clouds in the plane of the sky. For the reason that all the eight clouds are located very close to us ($\lesssim 200$ pc), we did not correct for any foreground contribution to the measured polarization. In this context, previous magnetic field studies by Soam et al. (2017, 2018) also reported no significant change in the polarization properties due to line-of-sight contribution for the clouds which are at distances closer than 500 pc.

The projected magnetic field geometries traced by the R-band polarization results (B_R) are presented on the *Herschel* 250 μ m images containing the clouds L1512, L1523, L1333, L1521E, L1517,

L1544, L1780 and L183 in Fig. 4. Since L1523 and L1333 were not observed with the *Herschel* telescope, we overplotted the polarization results on the *Dobashi* extinction map for these clouds as shown in Fig. 1 (second and third panel). The values of θ_{op} that are less than twice the standard deviation about the mean are plotted in the respective panels of Fig. 4 using the lines drawn in cyan and those greater than twice that value are shown using the lines drawn in green. The projected magnetic field traced using the *Planck* polarization vectors (B_{Plk}) are represented using the vectors drawn in yellow in all the panels of Fig. 4. The length of the vectors corresponds to the values of P_{op} and the direction corresponds to the θ_{op} measured from the north increasing towards the east.

The optical polarization traces the field lines towards the outer low-density regions of the cloud along particular line-of-sight (Franco et al. 2010; Sugitani et al. 2011; Saha et al. 2021) and the *Planck* polarization is more efficient in tracing the field orientations towards the denser parts of the cloud (Planck Collaboration et al. 2016). Therefore, ideally we should use R-band polarization measurements to trace magnetic field geometry towards the low-density extended regions of the eight clouds studied here and the *Planck* polarization measurements to trace the field lines towards the highdensity cores of the clouds. However, as can be seen from the Fig. 4, the R-band polarization measurements are for sources that are located around the immediate neighbourhood of the clouds while the *Planck* polarization measurements are available for the full extent of the clouds. It is worth noticing here that the sizes of the dense cores are typically $\sim 3-4'$ and the resolution of *Planck* data we used here is ~ 8 arcmin. Therefore, the *Planck* data traces the large-scale magnetic field towards the centre of the core, not the core scale magnetic fields. Since the polarized emission from dust grains given by *Planck* data is weighted by column density (Planck Collaboration et al. 2016) and we have considered the mean *Planck* polarization angle as the average of nearest vectors within an 8 arcmin region around the core centre, the θ_{plk} still represents the large scale magnetic fields around the core in this paper. The advantage of using the R-band polarization of the stars is that as we know the distances of the individual stars and the majority of those stars towards all the eight clouds are located at the background, we are certain that the measured polarization is actually due to the dust grains belonging to the cloud and hence traces the field geometry towards the clouds. Thus, the projected magnetic field directions traced by the R-band polarization measurements can be compared with those from the *Planck* measurements towards the low-density outer regions of the cloud. This is because the polarization detected in R-band is caused by the dust grains due to selective absorption which also emit thermally and causes the polarization detected by the *Planck*. Hence the polarization measurements made in the R-band and the *Planck* should be consistent towards the low-density parts of the cloud. Such agreements between the polarization measurements made in the optical and in the sub- or milli-meter wavelengths are seen in other studies also (e.g., Ward-Thompson et al. 2009; Soler et al. 2016; Gu & Li 2019). In addition to this, since polarization in R-band gives field geometry with relatively higher spatial resolution in comparison to the Planck polarization measurements, the R-band results are used to examine field distortions at smaller scales. Below we discuss the results obtained for individual clouds.

4.1.1 L1512

With the distance of 140 pc (shown with dotted line in Fig. 3), it is clear that the majority of the stars observed by us in the direction of L1512 are background sources and hence are tracing the pro-

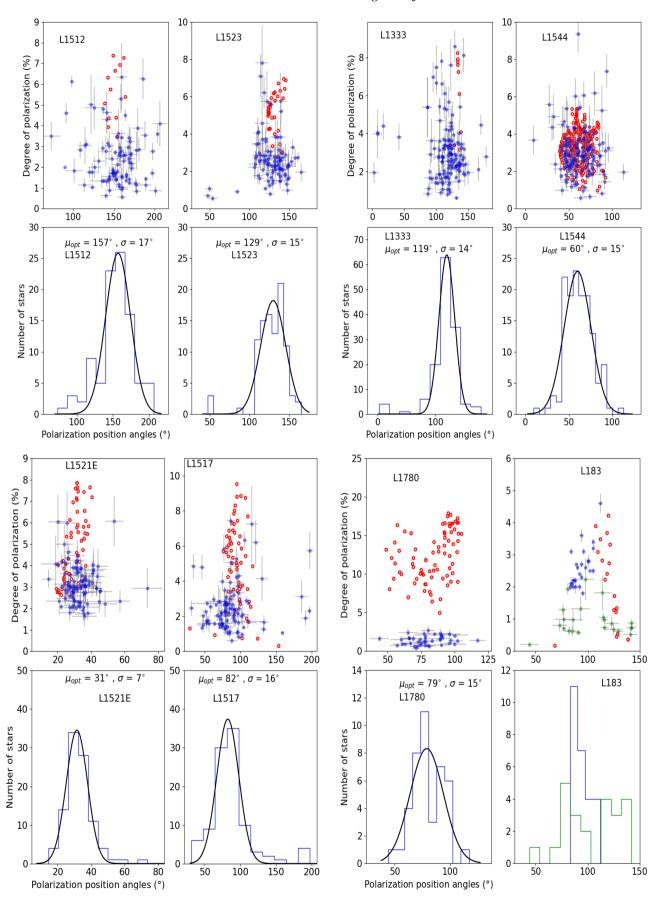


Figure 2. Top: Variation of the degree of polarization as a function of polarization position angle for L1512, L1523, L1333, L1544, L1521E, L1517, L1780 and L183. The blue and red symbols show our R-band and the *Planck* polarization results, respectively. Green filled circles and histogram show the H-polarization results from Clemens (2012). **Bottom:** Histogram of polarization angles from optical measurements.

Table 2. Basic information of the eight clouds studied here with results from the R-band and the Planck polarization measurements.

Cloud Id (1)	RA (J2000) (h:m:s) (2)	Dec (J2000) (d:m:s) (3)	Distance (pc) (4)	Ref. (5)	# of Stars Obs. (6)	P±e _p (%) (7)	$\theta_{op} \pm e_{op}$ (°) (8)	$\theta_{Plk} \pm e_{plk}$ (°) (9)
L1333	02:26:04	+75:28:30	170	5	137	3.0 ± 1.3	119±14	135±3
L1521E	04:29:21	+26:14:19	145^{+12}_{-16}	6	98	3.1 ± 0.8	31±7	30±6
L1517	04:55:45	+30:33:00	160±3	7	99	2.6 ± 1.4	82±16	93±19
L1512	05:04:09	+32:43:09	140 ± 20	1, 2	94	2.5 ± 1.3	157 ± 17	151±8
L1544	05:04:17	+25:10:48	130±6	8	136	3.0 ± 1.3	60 ± 15	61±11
L1523	05:06:14	+31:42:20	140	3, 4	97	2.7 ± 1.3	129 ± 15	131±7
L1780	15:39:42	-07:10:00	74	9, 10	41	1.4 ± 0.6	79 ± 15	84±15
L183	15:54:12	-02:49:42	115	9, 10	26	2.6 ± 0.6	94 ± 8	120 ± 14

1. Elias (1978), 2. Benson & Myers (1989), 3. Myers et al. (1983), 4. Wu et al. (1992), 5. Obayashi et al. (1998), 6. Yan et al. (2019), 7. Bailer-Jones et al. (2018), 8. Zucker et al. (2020), 9. Zucker et al. (2019), 10. Neha et al. (2018).

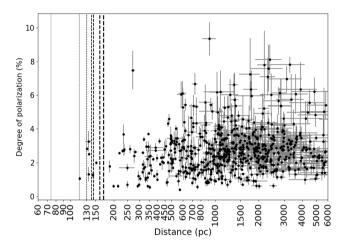


Figure 3. The variation of the fraction of polarization (P%) versus distance. The dotted lines show the known distances of all the eight clouds.

jected magnetic field geometry of the cloud as shown in Fig. 4 (Left top). The orientations of the $B_R\,$ and the $B_{Plk}\,$ are in excellent agreement (both showing an orientation of 158°). The consistency of the B_R and the B_{Plk} is even higher when we compare the θ_{op} within two standard deviation about the mean as shown by the vectors drawn in cyan. Since the optical polarization traces the field lines towards the outer low-density regions of the cloud and the Planck polarization is more efficient in tracing the field orientations towards the denser parts of the cloud, the agreement seen here suggests that the cloud is threaded by the same magnetic field from outer low-density medium to the high density regions of L1512. The projected field is aligned along the morphology of the cloud which is elongated in the northern direction. There is a curvature in the field lines along the northwest and southeast direction. The field lines are found to be tracing the two filaments seen to the western parts of the cloud. The degree of polarization (measured from both R-band and the *Planck*) is relatively lower towards the region with sharp edges as compared to the diffuse region on the opposite side. This could be due to the lack of aligned dust grains which may happen due to different grain size distribution or collisional disalignment with the gas (Soam et al. 2021). It could also be due to a tangled magnetic field causing depolarization (Planck Collaboration et al. 2015). The other reason might be that the magnetic field lines could be bending along the line of sight with a smaller component projected in the plane-of-the-sky.

4.1.2 L1523

The L1523 cloud shows a diffused tail towards the north-western parts of the cloud. The B_R (130°) and the B_{Plk} (132°) are found to be in excellent agreement in L1523 also indicating that the inner cloud magnetic field is inherited from the envelope magnetic field. Here again, the agreement is more pronounced as we consider the θ_{op} within two standard deviation about the mean as shown by the vectors drawn in cyan in Fig. 4 (top right). Both B_R and B_{Plk} show highly ordered distribution. The magnetic field orientation between the region to the south-eastern and the north-western parts of the cloud shows a small variation. It is at the position of the cloud where the change may be occurring. However, more data towards the northeastern parts of the cloud is required to make a definitive statement. Whether the change in the field orientation is caused because of the formation of the cloud or the formation of the cloud occurred because of the bend in the field created by the two components of the magnetic field is unclear. In the case of a weaker magnetic field, gas dynamics is not controlled by the field and hence forced to follow the motion of the gas. However, as the field strength increases, the field lines dominate the gas dynamics helping the clouds to remain coherent (Körtgen & Banerjee 2015).

4.1.3 L1333

The region, L1333, a nearby cloud in Cassiopeia at 180 pc (Obayashi et al. 1998), is considered to be an extreme environment of star-formation where a few low-mass stars are present in the filamentary cloud. The cloud presents an extended morphology towards the north-west and high density part towards the south-east. The field lines from $B_{\rm Plk}$ (135 °) are well correlated with the B_R (119 °) although there is more variation present in B_R towards the south-west side accounting for higher dispersion in the polarization angles. The field lines are again aligned along the direction of extended emission towards north-west as seen in Dobashi extinction map. It harbours a starless core at the southern part of the cloud shown by black ellipse which is well studied using multiple molecular lines (Lee & Myers 2011; Sohn et al. 2007; Park et al. 2004). The large-scale magnetic field is perpendicular to the orientation of the core.

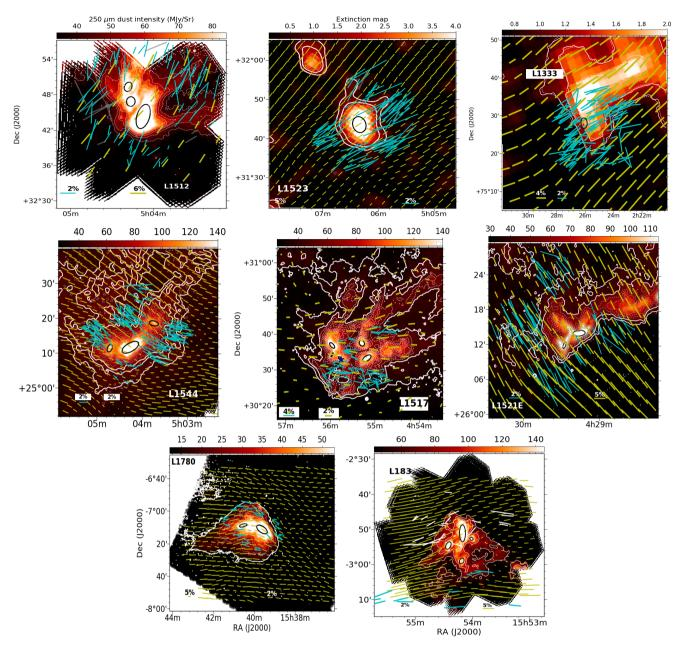


Figure 4. Optical R-band polarization vectors in cyan and *Planck* polarization measurements in yellow color overplotted on *Herschel* 250 μm image of L1512, L1544, L1517, L1521E, L1780 and L183 clouds and on *Dobashi* extinction map of L1523 and L1333 clouds. White vectors in bottom right last panel are H-band polarization observations for L183 (Clemens 2012). Distribution of the extracted cores identified using the *Astrodendro* algorithm shown by black ellipses.

4.1.4 L1544

The cloud L1544, one of the dark clouds hosting a starless core in Taurus (Myers et al. 1983; Heyer et al. 1987), with unusual chemical richness (Lee et al. 2003; Bizzocchi et al. 2014), offers a key laboratory to test physical conditions and stability of gas in starless cores. The $B_R \ (60^\circ)$ shown in cyan vectors are found to be in excellent agreement with the $B_{Plk} \ (61^\circ)$ implying that the field lines inside the cloud are preserved with the fields from the envelope of the cloud. Both B_R and B_{Plk} are mostly oriented perpendicular to the high density emission structures seen towards the cloud. The JCMT-SCUBA polarization maps of 850 μm thermal emission from dust in L1544 were obtained by Ward-Thompson et al. (2000). The mean

position angle of the magnetic field inferred is found to be at an offset of 23° with the B_R and $\sim 37^\circ$ with $B_{Plk}.$ It is interesting to note that towards the southern tip of the cloud both optical and the Planck polarization values show a change in the field direction from $\sim\!60^\circ$ to $\sim\!90^\circ.$ The degree of polarization shows a drop at this location consistently in measurements made in both the techniques. The magnetic fields orientation towards the diffuse extended region is found to be more parallel to the elongated morphology of the cloud in the north eastern direction. More details on the magnetic fields using optical polarization data will be discussed in Kumar & Soam 2022 (under preparation).

4.1.5 L1517

The L1517 cloud is relatively isolated only to be disturbed by the nearby pre-main sequence stars, AB Aurigae and SB Aurigae which are physically associated with the cloud (Heyer et al. 1987). The cores are at different evolutionary stages with detected N₂H⁺emission in selected cores. Fig. 4 shows that there is an excellent agreement between the field lines in the inner parts of the clouds (93°) to the field lines in the outer envelope (83°) of the cloud. Kirk et al. (2006) mapped the linear polarization emission from L1517B (one of the five cores in the cloud) at 850 μ m. The weighted mean of position angle was estimated as 106° which is at an offset of 13° with the B_{Plk} and at an offset of 23° from the B_R . Kirk et al. (2006) also reported a shift in the position angles from the north (84°) to the middle (94°) and to the southern parts (156°) of L1517B. It is evident from the Fig. 4, that there are changes in the large-scale magnetic field orientation around the cloud as found towards the north-east and south-west corners of the figure where field rotations are most likely causing a reduction in the degree of polarization possibly due to depolarization. Hacar & Tafalla (2011) have made a detailed study of L1517 in molecular lines and 1.2 mm dust continuum emission. They identified four filaments and five starless cores embedded in these filaments that are at different evolutionary stages. These filamentary structures stretch parallel to the direction of the extended emission and also to the direction of the magnetic fields. The magnetic fields towards the south of the cloud near AB Aur shown by blue star in Fig. 4) show more dis-oriented vectors with relatively large dispersion which could be because of the effects from this Herbig Ae star. Opposite to that, the vectors in the north of cloud show more ordered pattern.

4.1.6 L1521E

The cloud L1521E (Lee & Myers 1999) is considered to be chemically and dynamically young starless core in a larger cloud L1521 in Taurus constellation. The field orientations inferred from both the techniques are in excellent agreement implying that the magnetic field lines are preserved at core as well envelope scales in L1521E also. The field orientations follow the extended cloud structure of the cloud. The H₂ density at the peak position of the core is estimated to be $1.3-5.6\times10^5$ cm⁻³. However, although the H₂ density is such high enough to excite the inversion transitions of NH₃, these lines are found to be very faint in L1521E (Hirota et al. 2002). Tafalla & Santiago (2004) compared the emission of two molecules, C¹⁸O and N₂H⁺ which are known to have different depletion behaviours. While C¹⁸O gets heavily depleted at densities of a few 10⁴ cm⁻³, N_2H^+ remains at gas phase up to densities of $\sim 10^6$ cm⁻³. Thus, the ratio between the integrated intensities of $C^{18}O$ and $N_2H^{\scriptscriptstyle +}$ is a good indicator of depletion which is found to be 3.4 in L1521E implying that this core is chemically less processed and therefore youngest core known with a contraction age of $\lesssim 1.5 \times 10^5$ yr (Tafalla & Santiago 2004). However, this age is not compatible with the models of core formation via ambipolar diffusion, as they require evolutionary times of the order of 1 Myr. In that case, a more dynamical core formation scenario is required to create such a highly contracted core on a short time scale as estimated by using chemical models (Tafalla & Santiago 2004). The sharp edges to the southern side and a more extended distribution of material to the opposite direction could be a result of some external compression acted from the southern direction along the field lines that might have created the cloud.

4.1.7 L1780

The L1780 is a cometary shaped high cloud located at higher latitudes. For the case of L1780, the $B_R \ (77^\circ)$ and the $B_{Plk} \ (84^\circ)$ agree very well not only with respect to the mean orientation but also to the overall field morphology traced with the two techniques. The field lines remarkably follow the cloud structure. The cloud presents a cometary morphology with a broad high density part to the west and a diffuse narrow part to the east. The structure shows a curvature from east to west which is strikingly traced by the field lines as well. Towards the head, the degree of polarization is significantly lower compared to the other regions as traced by both the techniques.

4.1.8 L183

The morphology of L183 is directed towards south in form of Vshaped structure as shown by outer contours in Herschel emission (see Fig. 4). The R-band measurements made by us for cloud L183 are for the background stars lying towards the southern parts of the cloud while the H-band polarization measurements made by Clemens (2012) are for the background sources lying to the northern parts of the cloud. The magnetic fields inferred from the H-band polarization measurements made by Clemens (2012) are shown using the vectors drawn in white. Though the field orientations inferred from both R-band and H-band are in good agreement with the *Planck* polarization measurements, there are differences seen between the H-band and the *Planck* magnetic field orientations towards the western parts of the cloud where a reduction in the degree of polarization is seen. There could be two components of magnetic field orientation in this case which might be causing a depolarization resulting in the reduction of polarization. The maps generated using the R-, H- and Planck present a smooth and ordered field geometry over the entire field containing the cloud. The magnetic field is predominantly perpendicular to the north-south elongation of the cloud. The weighted mean position angle of the magnetic field, averaged over the 16 positions observed by Ward-Thompson et al. (2000) in 850 μ m is 46°. This represents the magnetic field geometry of the high density inner regions of the cloud which is at an offset of 74°, 57° and 48° with respect to the magnetic fields inferred by the Planck, H-band and R-band polarization measurements. This is the only cloud where we find the sharp edged northern and extended diffuse emission to the southern parts of the cloud are perpendicular to the magnetic field orientation. Karoly et al. (2020) has carried out the comparative study of the magnetic field structure of the cloud in optical, near-infrared wavelengths with sub-millimetre polarization using Pol-2 at JCMT. The authors have mapped the whole cloud using optical polarization. The mean value of magnetic field orientation is around ~ 87° using optical observations which is well consistent with our reported value.

5 DISCUSSION

We have studied the large-scale magnetic field structure of the clouds using *Planck* polarization and its small scale variations using optical polarization at the outer periphery of the cloud. The cloud magnetic fields are found to be parallel to inter-cloud magnetic fields in all the clouds. One common factor in all these selected clouds is their observed morphology. All the clouds show relatively bright rim on one side and the extended diffuse structure on the other side which can be noticed by the change in intensity along the elongation. We are interested in the direction of small intensity gradient in the cloud's

Table 3. Position angle of extended structure, magnetic field using R-band optical polarization and Planck polarization measurements.

Cloud Name	$ heta_{op}$ (°)	$ heta_{plk}$ (°)	$ heta_{env}$ (°)	$ heta_{plk}$ - $ heta_{env}$ (°)	$ heta_{op}$ - $ heta_{env}$
(1)	(2)	(3)	(4)	(5)	(6)
L1333	119	135	128	9	7
L1521E	31	30	43	12	13
L1517	82	93	136	54	43
L1512	157	151	148	9	3
L1544	60	61	36	24	25
L1523	129	131	137	8	6
L1780	79	84	100	21	16
L183	94	120	26	68	94

extended structure which is defined by θ_{env} . We visually selected directions from the brightest core in the map till the outer isocontours and calculated the gradient within the outer intensity isocontours. Hence, θ_{env} was extracted by taking the slowest change of intensity out of many selected directions. Table 3 shows the comparison between the magnetic field orientation (optical and *Planck*) with the structure of the cloud (θ_{env}). Our results suggest that the magnetic field lines in six clouds are almost oriented along the diffuse extended emission which is opposite the sharp edge of the cloud. One of the clouds, L183 which do not shows parallel orientation, showed almost same value of gradient in all the directions but different orientations. Kim et al. (2016) investigated a sample of starless cores using Akari emission maps and molecular line observations to conclude that the external feedback from the stars or the isotropic interstellar radiation field might play a crucial role in the evolution of the cores. In that study, L1512 and L1517B have been studied in detail using 3-160 μ m emission and they are found to be affected by the presence of star in their vicinity. This could be responsible for the asymmetric shape of the far-infrared emission in L1512 and L1517. The fact that the magnetic fields in this study are along the elongation of cloud structure in majority of the clouds may suggest a link to the feedback or effect from the ISRF. Vázquez-Semadeni et al. (2011) has suggested that the scenario of cloud formation is driven by colliding flows which can be guided by magnetic field and thereby facilitate the formation of filaments and fragmentation to the clumps/cores. The origin of these flows is still unknown. One possible explanation for the B-field aligned along the extended emission of the clouds is that the feedback from the stars nearby to the clouds might have stripped the clouds shown here.

5.1 Magnetic field strength and cloud stability

The Davis-Chandrasekhar-Fermi (DCF) method (Davis & Greenstein 1951; Chandrasekhar & Fermi 1953) is an effective means of estimating magnetic field strength by taking into account the dispersion in polarization angles and the non-thermal gas motions which are responsible to distort the magnetic field structure at smaller scales and also measure mass-to-flux ratio.

We used the following equation to calculate the strength of the plane-of-the-sky component of magnetic field:

$$\frac{B_{pos}}{(\mu G)} = 9.3 \times \sqrt{\frac{n_{H_2}}{cm^{-3}}} \times \frac{\Delta v}{kms^{-1}} \times \left(\frac{\Delta \phi}{1^{\circ}}\right)^{-1}$$
 (4)

where Δv is the FWHM obtained from the Gaussian fitting to the CO spectra and $\Delta \phi$ is the dispersion in polarization angle in degrees.

We estimated the magnetic field strength for all the clouds by taking dispersion in polarization angles from the optical polarization data and velocity dispersion from the available molecular line data of ^{13}CO for all the sources from Lee et al. (2004). Using 2×10^3 cm $^{-3}$ as the average number density for all the clouds and the dispersion in polarization angle from table 2, the strength has been calculated as \sim 27 $\mu\text{G}, \sim$ 18 $\mu\text{G}, \sim$ 21 $\mu\text{G}, \sim$ 26 $\mu\text{G}, \sim$ 23 μG and \sim 78 μG for L1333, L1512, L1523, L1544, L1517 and L1521E, respectively. The magnetic field strength for high-latitude clouds, L1780 and L183 were estimated as 11 μG and 42 μG by Neha et al. (2016). Assuming typical uncertainty in the velocity dispersion and the polarization angles, the uncertainty in the magnetic field strength is estimated to be \sim 0.5 B_{pos} .

The relative importance of the magnetic fields with respect to the self-gravity can be understood by calculating the mass-to-flux ratio which can tell whether or not magnetic fields are strong enough to support a molecular cloud against gravitational collapse (Mouschovias & Spitzer 1976). This can be quantified by a parameter (Crutcher 2004; Nakano & Nakamura 1978), $\lambda = 7.6 \times 10^{-21}$ $N_{H_2}/B_{\it pos}$ where N_{H_2} is the column density in units of cm⁻² and B_{pos} is the magnetic field strength in μ G. The mass-to-flux ratio has been calculated for all the sources to discuss the magnetic criticality/stability. If $\lambda > 1$, the cloud envelope is magnetically supercritical implying that the magnetic fields cannot support enough the cloud against gravitational collapse. Whereas if $\lambda < 1$, it is magnetically sub-critical implying the magnetic fields can prevent the gravitational collapse of the cloud. We took the extinction values from GAIA DR3 measurements for the stars observed in optical polarization observations. Using an average value of extinction for each cloud, we estimated the column density for all the clouds as 1.95, 1.96, 1.95, 2.56, 2.22, 1.69 (× 10^{21}) cm⁻² using the relation as N_{H₂} $(cm^{-2}) = 0.93 \times 10^{21} A_v$ (mag) (Bohlin et al. 1978). We estimated the values of mass-to-flux ratio as 0.55, 0.83, 0.71, 0.75, 0.73, 0.16 for the clouds L1333, L1512, L1523, L1544, L1517 and L1521E, respectively. By adopting the column density as 1×10^{21} (Montillaud et al. 2015), we estimated λ to be 0.7 and 0.18 for L1780 and L183, respectively. Since both L1780 and L183 are high latitude clouds and are at similar galactic latitude, we used the same column density for L183 also. Considering the uncertainty in the values of magnetic field strength, all the clouds are approaching the critical value except L1333, L1521E and L183. This implies that the magnetic fields are marginally supporting the cloud envelope against the self-gravity and are likely to play a significant role in governing the cloud dynamics. The very low values of L1333, L1521E and L183 indicate that the magnetic fields are strong enough to dominate the gas dynamics in the cloud envelope and can delay the gravitational collapse.

5.2 Relative orientation between the magnetic field and the core orientations

The star-forming cores or starless cores are considered to be the consequences of fragmentation of the clouds. Magneto-hydrodynamic simulations carried out by various authors Seifried et al. (2020); Heitsch et al. (2009) showed that the there is a significant change of magnetic field orientation (from low to high field strengths) in the formation of clouds. As the relative orientation of filaments and B-field are correlated in nearby cloud complexes (Soler & Hennebelle 2017), the cores, being the nested structures, will have effect from the magnetization of the cloud. In this regard, the clump shapes and the orientations are important indicators of clump dynamics and fate of star formation. The core-background magnetic field can provide important clues about the dynamical importance of magnetic field at the cloud scale in comparison to stellar feedback or turbulent

motions. In the previous section, we discussed the magnetic field orientation with respect to the distribution of the material around the clouds. In this section, we investigate the relative orientation between the core major axis and the ambient and the core-scale magnetic fields. Since the R-band polarization measurements trace the envelope magnetic fields or the fields at the periphery of the clouds, we define this as the ambient (θ_{op}) magnetic fields. The core-scale magnetic field defined by θ_{plk} is calculated by taking an average of the nearest three Planck polarization vectors around the inner regions of the cloud. The $\theta_{\textit{plk}}$ thus obtained are listed in the column 6 of Table 4. The positions of the cores associated with the selected clouds and their properties are obtained using the python package Astrodendro algorithm (Rosolowsky et al. 2008) on Herschel 250 μm emission maps. The dendrogram method identifies emission features at successive isocontours in emission maps which are called "leaves" and then find the intensity values at which they merge with the neighbouring structures (branches and trunks). We supplied an emission threshold above which all the structures are identified and contour intervals which decides the boundary between the distinct structures. The initial threshold and the contour step size were selected as a multiple of the σ , the rms of the intensity map. In our analysis, we are interested in the dense cores which are identified as leaves.

For each core, the dendrogram method estimated the core positions, the major and the minor axes, the effective radius of the core, and the position angle in degrees which is measured counterclockwise from the positive x-axis. The core major and minor axes are calculated from the intensity-weighted second moment in the direction of the major axis or perpendicular to the major axis. The derived properties of the cores are presented in Table 4. A total of 19 cores were identified in six clouds studied here. The right ascension and the declination of the extracted cores are given in the columns 2 and 3. The column 4 gives the aspect ratios of the cores. The orientation of the major axis measured from the north increasing to the east is given in column 5. The sources having aspect ratio higher than 0.8 were removed from the analysis to consider only elongated cores (Chen et al. 2020). The smallest structure that can be considered as real is of size ~ 0.75 FWHM (Miville-Deschênes et al. 2017). We selected only those sources where the derived radius is larger than 2-3 pixels with the beam size of 250 μ m intensity map. In addition to these, we considered only those sources lying within the asymmetric structure of the cloud (shown by white contours in fig. 4 (right panel)). A total of 19 cores are identified in six clouds studied here, five cores in L1517, four in L183, three each in L1512 and L1544, two each in L1521E and L1780. We adopted the positions and major axis orientation of the cores in L1523 and L1333 from Lee & Myers (1999) as there are no Herschel maps available. The extracted cores in each cloud are shown in the panels of Fig. 4. In L1512, the major axis of the three extracted cores are almost parallel to each other and parallel to the ambient magnetic field. Interestingly, the core major axis orientation is along the elongated morphology of the cloud. In contrast, in L183, the major axes of three of the four cores are oriented parallel to each other, but perpendicular to the ambient magnetic field.

In Fig. 5, we show the distribution of the angle offset between the direction of core major axes with respect to the magnetic field from Planck, $|\theta_{plk} - \theta_{maj}|$ in left panel and the magnetic field from R-band polarization, $|\theta_{op} - \theta_{maj}|$ in right panel. If the core orientation has a significant effect due to the large-scale magnetic field, we expect the core major axis to be perpendicular to the magnetic field lines with a significant effect on the gas motions. Contrary to this, in the Fig. 5, we find that all the cores extracted show a random orientation

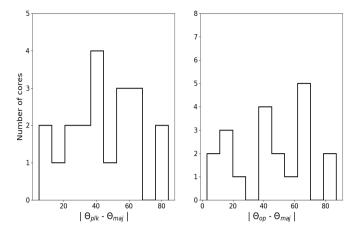


Figure 5. Left: Distribution of the difference of inner magnetic field and position angle of major axis. **Right:** Difference of outer magnetic field and position angle of major axis.

with respect to the outer (R-band) as well inner (*Planck*) magnetic field. We quantified our inference using a statistical technique, the *Rayleigh circular statistic* which gives a measure of relative alignment of structures with respect to the magnetic field and to obtain a statistical strength of that alignment (Jow et al. 2018). We define projected Rayleigh statistic (PRS) as

$$Z = \sum_{i=1}^{n} \cos \phi_i / \sqrt{n/2},\tag{5}$$

where ϕ_i = $2\theta_i$ and θ_i is the offset between the magnetic field and core major axes. If Z « 0, it is considered to be parallel alignment and if Z » 0, it is considered to be a perpendicular alignment. If Z≈ 0, the distribution is either random or preferentially lies around 45°. We have estimated Z to be 0.05 and -0.15 for *Planck* and R-band data, respectively. The offsets in both the cases are neither parallel nor perpendicular owing to the values close to zero and hence, follow random distribution. The same analysis was done by Jow et al. (2018) on the nearby Gould belt regions and Vela cloud to test the preferential alignment of column density structures with magnetic field and the values vary approximately from -5 to 5 to show transition from parallel to perpendicular alignment.

This result implies that the core orientation might not have a significant effect from the large-scale magnetic field as per the scenario of magnetic field dominated low mass star formation (Shu et al. 1987; Mouschovias & Ciolek 1999). There might be other factors that can contribute to shaping the core morphology such as feedback effects or the ram pressure as suggested by Chen & Ostriker (2018). Although we expect that the cores tend to align their major axis perpendicular to the local magnetic field where the flow of material will be preferential to favour the collapse mechanism, the environment can be a crucial effect towards the morphology of the cores. Chen & Ostriker (2018) showed that the environment also plays an important role in shaping the prestellar cores through ram pressure and magnetic pressure. The turbulence created by stellar feedback may affect the orientation of the cores' minor axis (Kim et al. 2016) or the local magnetization within the cloud (Chen et al. 2020).

Table 4. Position angle of cores, cloud magnetic field using R-band optical polarization and core-scale magnetic field Planck polarization measurements.

A		(b/a)	θ^{+} .	θ^c	$\Lambda \theta^{\rho i \kappa}$	$\Lambda \theta^{opi}$	Cores studied					
:m:s)	Dec (d:m:s)	(6/4)	θ_{maj}^{\ddagger} (°)	θ^c_{plk} (°)	$\Delta \theta_{maj}^{plk}$ (°)	$\Delta \theta_{maj}^{opt}$ (°)	in literature					
	(3)	(4)	(5)	(6)	(7)	(8)	(9)					
')	(3)	(+)	(3)	(0)	(7)	(0)	())					
L1333, $\theta_{op} = 119^{\circ} \pm 15^{\circ}$												
2:26:04	+75:28:30	0.18	2†	135	117	133	L1333 (1)					
	L	1521E,	$\theta_{op} = 32$	°±7°								
1:29:28	+26:11:60	0.35	159	37	58	51						
1:29:16	+26:14:05	0.45	94	31	63	64	L1521E (1)					
	Li	1517, θ_o	_{op} = 83°:	±14°								
1:55:11	+30:33:19			79	44	41	L1517B (1)					
1:55:47	+30:33:14	0.38	42	86	44	41	L1517A (1)					
1:55:57	+30:34:17	0.27	150	87	63	66	L1517C(1)					
1:55:58	+30:36:54	0.47	41	90	49	42						
1:55:18	+30:37:34	0.79	41	82	41	42						
	L1	512 , θ _{oj}	, = 158°	±16°								
5:04:07	+32:44:19			142	23	7	L1512-1 (1)					
5:04:16	+32:46:50	0.80	176	143	33	18						
5:04:18	+32:49:20	0.70	161	147	14	3						
	L	1544, θ_o	$p_p = 60^\circ$	±16°								
5:04:16	+25:11:44	0.45	118	60	58	58	L1544 (2)					
5:04:43	+25:11:25	0.62	153	69	84	87	L1544-E (2)					
5:03:45	+25:18:37	0.50	77	40	37	17	L1544-W (2)					
	L1	523 , θ _{οι}	$_{0} = 130^{\circ}$	±14°								
5:06:20	+31:43:33			126	67	64	L1523 (1)					
	L	1780 , θ _o	p = 79°:	±15°								
5:39:37	-07:11:20	0.46	61	68	7	17						
5:40:32	-07:08:52	0.33	102	97	5	23						
	I	L 183 , θ_o	p = 93°:	±8°								
5:54:11	-02:59:00	0.66	160	132	28	67						
5:54:25	-02:54:38	0.57	158	122	36	65						
5:54:10	-02:51:08	0.33	180	120	60	87	L183B (1)					
5:54:01	-02:52:42	0.85	42	126	84	51						
	::26:04 ::29:28 ::29:16 ::55:11 ::55:47 ::55:57 ::55:58 ::04:16 ::04:16 ::04:16 ::04:18 ::04:16 ::04:32 ::55:37 ::55:47 ::40:32	L1 ::26:04 +75:28:30 L29:28 +26:11:60 ::29:16 +26:14:05 L3::55:11 +30:33:19 ::55:47 +30:33:14 ::55:57 +30:34:17 ::55:58 +30:36:54 ::55:18 +30:37:34 L1 ::04:16 +32:44:19 ::04:16 +32:46:50 ::04:18 +32:49:20 L2::04:16 +25:11:25 ::03:45 +25:11:25 ::03:45 +25:11:25 ::03:45 +25:11:25 ::03:45 +25:11:20 ::40:32 -07:08:52 L3::54:11 -02:59:00 ::54:25 -02:54:38 ::54:10 -02:51:08	L1333, θ_{op} L1521E, θ_{op} 2:29:28 +26:11:60 0.35 2:29:16 +26:14:05 0.45 L1517, θ_{op} 2:55:11 +30:33:19 0.49 2:55:47 +30:33:14 0.38 2:55:57 +30:34:17 0.27 2:55:58 +30:36:54 0.47 2:55:18 +30:37:34 0.79 L1512, θ_{op} 2:04:16 +32:44:19 0.47 2:04:16 +32:46:50 0.80 2:04:18 +32:49:20 0.70 L1544, θ_{op} 2:04:16 +25:11:44 0.45 2:04:16 +25:11:25 0.62 2:03:45 +25:18:37 0.50 L1780, θ_{op} 2:1780, θ_{op} 2:1780, θ_{op} 2:183, θ_{op} 3:39:37 -07:11:20 0.46 3:40:32 -07:08:52 0.33 L183, θ_{op} 3:54:11 -02:59:00 0.66 3:54:25 -02:54:38 0.57 3:55:10 -02:51:08 0.33	L1333, $\theta_{op} = 119^{\circ}$ L1521E, $\theta_{op} = 32$ 2:29:28 +26:11:60 0.35 159 2:29:16 +26:14:05 0.45 94 L1517, $\theta_{op} = 83^{\circ}$ 2:55:11 +30:33:19 0.49 123 2:55:47 +30:33:14 0.38 42 2:55:57 +30:34:17 0.27 150 2:55:58 +30:36:54 0.47 41 2:55:18 +30:37:34 0.79 41 L1512, $\theta_{op} = 158^{\circ}$ 2:04:16 +32:44:19 0.47 165 2:04:16 +32:46:50 0.80 176 2:04:16 +32:49:20 0.70 161 L1544, $\theta_{op} = 60^{\circ}$ 3:04:16 +25:11:44 0.45 118 3:04:43 +25:11:25 0.62 153 3:03:45 +25:18:37 0.50 77 L1523, $\theta_{op} = 130^{\circ}$ 2:06:20 +31:43:33 0.73 13† L1780, $\theta_{op} = 79^{\circ}$ 3:39:37 -07:11:20 0.46 61 3:40:32 -07:08:52 0.33 102 L183, $\theta_{op} = 93^{\circ}$ 2:54:11 -02:59:00 0.66 160 3:54:25 -02:54:38 0.57 158 3:55:10 -02:51:08 0.33 180	L1333, $\theta_{op} = 119^{\circ} \pm 15^{\circ}$ L1521E, $\theta_{op} = 32^{\circ} \pm 7^{\circ}$ 1:29:28	L1333, $\theta_{op} = 119^{\circ} \pm 15^{\circ}$ L1521E, $\theta_{op} = 32^{\circ} \pm 7^{\circ}$ E29:28 +26:11:60 0.35 159 37 58 E29:16 +26:14:05 0.45 94 31 63 L1517, $\theta_{op} = 83^{\circ} \pm 14^{\circ}$ E55:11 +30:33:19 0.49 123 79 44 E55:47 +30:33:14 0.38 42 86 44 E55:57 +30:34:17 0.27 150 87 63 E55:58 +30:36:54 0.47 41 90 49 E55:18 +30:37:34 0.79 41 82 41 L1512, $\theta_{op} = 158^{\circ} \pm 16^{\circ}$ E04:16 +32:44:19 0.47 165 142 23 E04:16 +32:44:19 0.47 165 142 23 E04:16 +32:46:50 0.80 176 143 33 E04:18 +32:49:20 0.70 161 147 14 L1544, $\theta_{op} = 60^{\circ} \pm 16^{\circ}$ E04:43 +25:11:25 0.62 153 69 84 E04:43 +25:11:25 0.62 153 69 84 E1523, $\theta_{op} = 130^{\circ} \pm 14^{\circ}$ E1523, $\theta_{op} = 130^{\circ} \pm 14^{\circ}$ E1523, $\theta_{op} = 130^{\circ} \pm 14^{\circ}$ E166:20 +31:43:33 0.73 13† 126 67 L1780, $\theta_{op} = 79^{\circ} \pm 15^{\circ}$ E139:37 -07:11:20 0.46 61 68 7 E106:20 +31:43:33 0.73 13† 126 67 E183, $\theta_{op} = 93^{\circ} \pm 8^{\circ}$ E154:11 -02:59:00 0.66 160 132 28 E154:25 -02:54:38 0.57 158 122 36 E55:510 -02:51:08 0.33 180 120 60	L1333, $\theta_{op} = 119^{\circ} \pm 15^{\circ}$ L1521E, $\theta_{op} = 32^{\circ} \pm 7^{\circ}$ 129:28					

[‡] Position angle of the major axis of the cores. $\Delta \theta_{maj}^{pla} = |\theta_{pla} - \theta_{maj}|, \Delta \theta_{maj}^{opt} = |\theta_{opt} - \theta_{maj}|$

6 CONCLUSIONS

In this work, we presented our R-band polarization measurements of over 500 stars projected on eight small, isolated clouds. Of these, we took observations for six of these clouds, namely, L1512, L1523, L1333, L1521E, L1517 and L1544. These sources were chosen on the basis of their cloud morphology from *Herschel* 250 μ m emission or *Dobashi* extinction map having sharp edges on one side and an extended emission on the opposite direction to trace the plane-of-the-sky magnetic field geometry of these clouds. Two more clouds, L1780 and L183, showing this emission were added to the sample from the literature. The main goals of the study are (a) to investigate the relationship between the observed magnetic field orientation with respect to the elongated morphology seen in the clouds; (b) to investigate the relationship between the magnetic field orientations inside the clouds inferred from the *Planck* polarization and the envelope-scale field inferred from the optical polarization mea-

surements of background starlight; (c) to examine the relative offsets between the core major axes orientation with respect to both inner and outer magnetic field directions. The results obtained from this study are given below:

- (i) Based on the distribution of the degree of polarization and the position angles of the stars projected on all the eight clouds (measured by us in R-band and taken from archival data) with respect to the distances of the stars obtained from the *Gaia* EDR3, we show evidence that all the stars are found to be located at distance farther than ~ 200 pc.
- (ii) In all the eight clouds studied here, the magnetic fields inferred from the R-band polarization and the *Planck* polarization measurements are in excellent agreement, suggesting that it is the same dust population which is possibly responsible for the production of polarization that is detected in the two techniques.
 - (iii) In seven out of eight clouds studied, the projected magnetic

[†] Value of major axes have been taken from Lee & Myers (1999). 1. Lee et al. (1999), 2. Tafalla et al. (1998)

field is aligned with the direction of diffuse emission of cloud. The one cloud, L183, has its diffuse emission oriented perpendicular to the ambient magnetic field.

- (iv) The magnetic field strength estimated with DCF method in all the clouds ranges from 11-78 μ G. With the column density and the derived field strength, we calculated the mass-to-flux ratio, λ with the values ranging from 0.16-0.83. Except L1333, L1521E, and L183 all the clouds show magnetically critical state suggesting that the magnetic pressure are almost supporting the gravity in the cloud envelope.
- (v) A total of 19 cores are extracted from the six clouds. The major axes of the three cores found in L1512 from Herschel 250 µm emission are not only found to be parallel to each other but also to both the projected magnetic fields and the direction of diffuse emission of the cloud. In contrast, for three out of four cores in L183, their major axes are found to be parallel to each other and also to the cloud elongation, but almost perpendicular to the orientation of the ambient magnetic field.
- (vi) The orientation of the core major axis with respect to the (projected) ambient and the inner magnetic fields is randomly distributed.

ACKNOWLEDGEMENTS

We thank all the supporting staff at 104-cm Sampurnanand Telescope, ARIES, Nainital who had provided assistance in carrying out these observations. This research has made use of the SIMBAD database, operated at CDS, Strasbourg, France. We also acknowledge the use of NASA's SkyView facility (http://skyview.gsfc.nasa.gov) located at NASA Goddard Space Flight Center. This work has made use of data from the following sources: (1) European Space Agency (ESA) mission Gaia (https: //www.cosmos.esa.int/gaia), processed by the Gaia Data Processing and Analysis Consortium (DPAC, https://www.cosmos. esa.int/web/gaia/dpac/consortium). Funding for the DPAC has been provided by national institutions, in particular the institutions participating in the Gaia Multilateral Agreement; (2) the Planck Legacy Archive (PLA) contains all public products originating from the *Planck* mission, and we take the opportunity to thank ESA/Planck and the Planck collaboration for the same; (3) the Herschel SPIRE images from Herschel Science Archive (HSA). Herschel is an ESA space observatory with science instruments provided by European-led Principal Investigator consortia and with important participation from NASA. C.W.L is supported by the Basic Science Research Program (2019R1A2C1010851) through the National Research Foundation of Korea. Some of the results in this paper have been derived using the healpy and HEALPix package. This paper is based on one of the chapters of thesis by E. Sharma on "Investigation of the evolution of dark clouds" (http: //hdl.handle.net/2248/7861).

DATA AVAILABILITY

The Gaia distances of the stars are available at https: //vizier.u-strasbg.fr/viz-bin/VizieR-3?-source= I/350/gaiaedr3. The Herschel maps are available at Herschel science archive (http://archives.esac.esa.int/hsa/whsa/). The optical polarization data is given in the appendices below.

REFERENCES

```
Alves F. O., Franco G. A. P., Girart J. M., 2008, A&A, 486, L13
Alves F. O., Frau P., Girart J. M., Franco G. A. P., Santos F. P., Wiesemeyer
    H., 2014, A&A, 569, L1
André P., et al., 2010, A&A, 518, L102
Bailer-Jones C. A. L., Rybizki J., Fouesneau M., Mantelet G., Andrae R.,
    2018, AJ, 156, 58
Bailer-Jones C. A. L., Rybizki J., Fouesneau M., Demleitner M., Andrae R.,
    2021, AJ, 161, 147
Bailey N. D., Basu S., Caselli P., 2017, A&A, 601, A18
Ballesteros-Paredes J., Klessen R. S., Mac Low M. M., Vazquez-Semadeni
    E., 2007, in Reipurth B., Jewitt D., Keil K., eds, Protostars and Planets
    V. p. 63 (arXiv:astro-ph/0603357)
Banerjee R., Vázquez-Semadeni E., Hennebelle P., Klessen R. S., 2009, MN-
    RAS, 398, 1082
Basu S., Mouschovias T. C., 1995, ApJ, 453, 271
Benson P. J., Myers P. C., 1983, ApJ, 270, 589
Benson P. J., Myers P. C., 1989, ApJS, 71, 89
Bizzocchi L., Caselli P., Spezzano S., Leonardo E., 2014, A&A, 569, A27
Bohlin R. C., Savage B. D., Drake J. F., 1978, ApJ, 224, 132
Chandrasekhar S., Fermi E., 1953, ApJ, 118, 113
Chen C.-Y., Ostriker E. C., 2014, ApJ, 785, 69
Chen C.-Y., Ostriker E. C., 2015, ApJ, 810, 126
Chen C.-Y., Ostriker E. C., 2018, ApJ, 865, 34
Chen C.-Y., et al., 2020, MNRAS, 494, 1971
Clemens D. P., 2012, ApJ, 748, 18
Commerçon B., Hennebelle P., Henning T., 2011, ApJ, 742, L9
Crutcher R. M., 2004, Ap&SS, 292, 225
Crutcher R. M., 2012, ARA&A, 50, 29
Davis Jr. L., Greenstein J. L., 1951, ApJ, 114, 206
Elias J. H., 1978, ApJ, 224, 857
Franco G. A. P., Alves F. O., Girart J. M., 2010, ApJ, 723, 146
Gaia Collaboration et al., 2021, A&A, 649, A1
Goodman A. A., Bastien P., Menard F., Myers P. C., 1990, ApJ, 359, 363
Górski K. M., Hivon E., Banday A. J., Wandelt B. D., Hansen F. K., Reinecke
    M., Bartelmann M., 2005, ApJ, 622, 759
Gu Q., Li H.-b., 2019, ApJ, 871, L15
Hacar A., Tafalla M., 2011, A&A, 533, A34
Hatchell J., Richer J. S., Fuller G. A., Qualtrough C. J., Ladd E. F., Chandler
    C. J., 2005, A&A, 440, 151
Heitsch F., Stone J. M., Hartmann L. W., 2009, ApJ, 695, 248
Heyer M. H., Vrba F. J., Snell R. L., Schloerb F. P., Strom S. E., Goldsmith
    P. F., Strom K. M., 1987, ApJ, 321, 855
Heyer M., Gong H., Ostriker E., Brunt C., 2008, ApJ, 680, 420
Hiltner W. A., 1949, Nature, 163, 283
Hirota T., Ito T., Yamamoto S., 2002, ApJ, 565, 359
Inutsuka S.-I., Miyama S. M., 1992, ApJ, 388, 392
Jow D. L., Hill R., Scott D., Soler J. D., Martin P. G., Devlin M. J., Fissel
    L. M., Poidevin F., 2018, MNRAS, 474, 1018
Karoly J., Soam A., Andersson B. G., Coudé S., Bastien P., Vaillancourt J. E.,
    Lee C. W., 2020, ApJ, 900, 181
Kawada M., et al., 2007, PASJ, 59, S389
Kim G., Lee C. W., Gopinathan M., Jeong W.-S., Kim M.-R., 2016, ApJ,
Kirk J. M., Ward-Thompson D., Crutcher R. M., 2006, MNRAS, 369, 1445
Klessen R. S., Hennebelle P., 2010, A&A, 520, A17
Körtgen B., Banerjee R., 2015, MNRAS, 451, 3340
Kudoh T., Basu S., 2011, ApJ, 728, 123
Launhardt R., et al., 2013, A&A, 551, A98
Lazarian A., 2007, J. Quant. Spectrosc. Radiative Transfer, 106, 225
Lee C. W., Myers P. C., 1999, ApJS, 123, 233
Lee C. W., Myers P. C., 2011, ApJ, 734, 60
Lee C. W., Myers P. C., Tafalla M., 1999, ApJ, 526, 788
Lee J.-E., Evans Neal J. I., Shirley Y. L., Tatematsu K., 2003, ApJ, 583, 789
Lee C. W., Myers P. C., Plume R., 2004, ApJS, 153, 523
Li H.-B., Blundell R., Hedden A., Kawamura J., Paine S., Tong E., 2011,
```

MNRAS, 411, 2067

- Li H. B., Goodman A., Sridharan T. K., Houde M., Li Z. Y., Novak G., Tang K. S., 2014, in Beuther H., Klessen R. S., Dullemond C. P., Henning T., eds, Protostars and Planets VI. p. 101 (arXiv:1404.2024), doi:10.2458/azu_uapress_9780816531240-ch005
 Li H.B. Jiang H. Fan X. Gu Q. Zhang Y. 2017. Nature Astronomy. 1
- Li H.-B., Jiang H., Fan X., Gu Q., Zhang Y., 2017, Nature Astronomy, 1, 0158
- Lindegren L., et al., 2021, A&A, 649, A2
- McKee C. F., Ostriker E. C., 2007, ARA&A, 45, 565
- Miville-Deschênes M. A., et al., 2017, A&A, 599, A109
- Montillaud J., et al., 2015, A&A, 584, A92
- Mouschovias T. C., Ciolek G. E., 1999, in Lada C. J., Kylafis N. D., eds, NATO Advanced Study Institute (ASI) Series C Vol. 540, The Origin of Stars and Planetary Systems. p. 305
- Mouschovias T. C., Spitzer Jr. L., 1976, ApJ, 210, 326
- Myers P. C., Benson P. J., 1983, Rev. Mex. Astron. Astrofis., 7, 238
- Myers P. C., Linke R. A., Benson P. J., 1983, ApJ, 264, 517
- Nakamura F., Li Z.-Y., 2011, ApJ, 740, 36
- Nakano T., Nakamura T., 1978, PASJ, 30, 671
- Neha S., Maheswar G., Soam A., Lee C. W., Tej A., 2016, A&A, 588, A45
- Neha S., Maheswar G., Soam A., Lee C. W., 2018, MNRAS, 476, 4442
- Nielbock M., et al., 2012, A&A, 547, A11
- Nutter D., Stamatellos D., Ward-Thompson D., 2009, MNRAS, 396, 1851
- Obayashi A., Kun M., Sato F., Yonekura Y., Fukui Y., 1998, AJ, 115, 274
- Palau A., et al., 2013, ApJ, 762, 120
- Park Y.-S., Lee C. W., Myers P. C., 2004, ApJS, 152, 81
- Planck Collaboration et al., 2015, A&A, 576, A104
- Planck Collaboration et al., 2016, A&A, 586, A138
- Poidevin F., et al., 2014, ApJ, 791, 43
- Rautela B. S., Joshi G. C., Pandey J. C., 2004, Bulletin of the Astronomical Society of India, 32, 159
- Rosolowsky E. W., Pineda J. E., Kauffmann J., Goodman A. A., 2008, ApJ, 679, 1338
- Saha P., Gopinathan M., Sharma E., Won Lee C., Ghosh T., Kim S., 2021, A&A, 655, A76
- Schmidt G. D., Elston R., Lupie O. L., 1992, aj, 104, 1563
- Seifried D., Walch S., Weis M., Reissl S., Soler J. D., Klessen R. S., Joshi P. R., 2020, MNRAS, 497, 4196
- Sharma E., et al., 2020, A&A, 639, A133
- Shu F. H., Adams F. C., Lizano S., 1987, ARA&A, 25, 23
- Soam A., Maheswar G., Bhatt H. C., Lee C. W., Ramaprakash A. N., 2013, MNRAS, 432, 1502
- Soam A., Maheswar G., Lee C. W., Dib S., Bhatt H. C., Tamura M., Kim G., 2015, A&A, 573, A34
- Soam A., Lee C. W., Maheswar G., Kim G., Neha S., Kim M.-R., 2017, MNRAS, 464, 2403
- Soam A., Maheswar G., Lee C. W., Neha S., Kim K.-T., 2018, MNRAS, 476,
- Soam A., et al., 2021, AJ, 161, 149
- Sohn J., Lee C. W., Park Y.-S., Lee H. M., Myers P. C., Lee Y., 2007, ApJ, 664, 928
- Soler J. D., Hennebelle P., 2017, A&A, 607, A2
- Soler J. D., et al., 2016, A&A, 596, A93
- Sugitani K., et al., 2010, ApJ, 716, 299
- Sugitani K., et al., 2011, ApJ, 734, 63
- Tafalla M., Santiago J., 2004, A&A, 414, L53
- Tafalla M., Mardones D., Myers P. C., Caselli P., Bachiller R., Benson P. J., 1998, ApJ, 504, 900
- Vázquez-Semadeni E., Banerjee R., Gómez G. C., Hennebelle P., Duffin D., Klessen R. S., 2011, MNRAS, 414, 2511
- Vrba F. J., Strom S. E., Strom K. M., 1976, AJ, 81, 958
- Ward-Thompson D., Scott P. F., Hills R. E., Andre P., 1994, MNRAS, 268,
- Ward-Thompson D., Kirk J. M., Crutcher R. M., Greaves J. S., Holland W. S., André P., 2000, ApJ, 537, L135
- Ward-Thompson D., Sen A. K., Kirk J. M., Nutter D., 2009, MNRAS, 398,
- Wu Y., Zhou S., Evans Neal J. I., 1992, ApJ, 394, 196

- Yan Q.-Z., Zhang B., Xu Y., Guo S., Macquart J.-P., Tang Z.-H., Walsh A. J., 2019, A&A, 624, A6
- Zonca A., Singer L., Lenz D., Reinecke M., Rosset C., Hivon E., Gorski K., 2019, Journal of Open Source Software, 4, 1298
- Zucker C., Speagle J. S., Schlafly E. F., Green G. M., Finkbeiner D. P., Goodman A. A., Alves J., 2019, ApJ, 879, 125
- Zucker C., Speagle J. S., Schlafly E. F., Green G. M., Finkbeiner D. P., Goodman A., Alves J., 2020, A&A, 633, A51

APPENDIX A: TABLES

The Color	
L1333 1 36.635574 75.557785 2.3±0.1 2 36.832424 75.556046 8.1±0.9 3 36.900402 75.564400 2.9±0.5 4 36.706692 75.534019 2.2±0.1 5 36.824272 75.548027 3.1±0.2 6 36.721371 75.522621 2.3±0.2 7 36.851704 75.535210 2.9±0.3 8 36.815571 75.524368 4.4±0.9 9 36.968765 75.533386 2.4±0.6 10 36.673347 75.487823 2.5±0.8 11 36.630009 75.478310 2.3±0.7 12 36.678047 75.479797 1.3±0.2 13 36.798355 75.495140 4.6±0.9 14 36.878319 75.495140 4.6±0.9 15 36.955891 75.505592 2.7±0.7 16 36.878319 75.49931 2.9±0.7 18 36.966125 75.497597 4.2±0.7	$\theta_{op} \pm e_{op}$ (°)
1 36.635574 75.557785 2.3±0.1 2 36.832424 75.556046 8.1±0.9 3 36.900402 75.560440 2.9±0.5 4 36.706692 75.534019 2.2±0.1 5 36.824272 75.548027 3.1±0.2 6 36.721371 75.522621 2.3±0.2 7 36.851704 75.535210 2.9±0.3 8 36.815571 75.524368 4.4±0.9 9 36.968765 75.533386 2.4±0.6 10 36.673347 75.487823 2.5±0.8 11 36.63009 75.478310 2.3±0.7 12 36.678047 75.479797 1.3±0.2 13 36.798355 75.495140 4.6±0.9 14 36.851345 75.496162 2.8±0.7 15 36.955891 75.505592 2.7±0.7 16 36.878319 75.489311 2.9±0.2 17 36.939865 75.497597 4.2±0.7 18 36.966125 75.499939 2.6±0.2 19 36.497143 75.416504 1.1±0.3 20 36.552902 75.420486 1.7±0.3 21 36.792648 75.450446 1.7±0.3 22 36.801079 75.450340 1.8±0.3 23 36.717266 75.437553 3.4±0.5 24 36.688969 75.432884 3.0±0.4 25 36.687901 75.425781 3.5±0.5 26 36.526684 75.392769 2.6±0.2 27 36.536018 75.386826 5.4±1.6 28 36.536018 75.386826 5.4±1.6 29 36.818443 75.420723 1.4±0.1 30 36.753849 75.409576 3.7±0.6 31 36.633022 75.388786 2.3±0.5 32 36.642246 75.385384 3.2±0.3 33 36.749104 75.400932 1.9±0.6 34 36.802547 75.408531 2.9±0.7 35 36.739025 75.388786 2.3±0.5 36 36.682495 75.379448 2.4±0.5 37 36.665897 75.379448 2.4±0.5 38 36.816051 75.38626 5.4±1.6 29 36.818443 75.420723 1.4±0.1 30 36.753849 75.409576 3.7±0.6 31 36.633022 75.388786 2.3±0.5 32 36.642246 75.385384 3.2±0.3 33 36.749104 75.400932 1.9±0.6 34 36.802547 75.408531 2.9±0.7 35 36.739025 75.388939 2.5±0.3 36 36.682495 75.379448 2.4±0.5 37 36.665897 75.374657 2.9±0.6 40 36.828247 75.380699 2.8±0.2 41 36.441269 75.385460 2.5±0.3 44 36.718288 75.378220 1.5±0.5 45 36.507980 75.344017 2.0±0.6 46 36.482780 75.326973 2.8±0.6 47 36.543869 75.321381 1.4±0.4 48 36.667274 75.338501 1.6±0.1	
2 36.832424 75.5560466 8.1±0.9 3 36.900402 75.564400 2.9±0.5 4 36.706692 75.534019 2.2±0.1 5 36.824272 75.548027 3.1±0.2 6 36.721371 75.522621 2.3±0.2 7 36.851704 75.535210 2.9±0.3 8 36.815571 75.524368 4.4±0.9 9 36.968765 75.533386 2.4±0.6 10 36.673347 75.487823 2.5±0.8 11 36.630009 75.478310 2.3±0.7 12 36.678047 75.479797 1.3±0.2 13 36.798355 75.495140 4.6±0.9 14 36.851345 75.495140 4.6±0.9 15 36.878319 75.495140 4.6±0.9 16 36.878319 75.495140 4.6±0.9 17 36.939865 75.497597 4.2±0.7 18 36.966125 75.499939 2.6±0.5 19 36.4	
3 36.900402 75.564400 2.9±0.5 4 36.706692 75.534019 2.2±0.1 5 36.824272 75.548027 3.1±0.2 6 36.721371 75.522621 2.3±0.2 7 36.851704 75.535210 2.9±0.3 8 36.815571 75.524368 4.4±0.9 9 36.968765 75.533386 2.4±0.6 10 36.673347 75.487823 2.5±0.8 11 36.630009 75.478310 2.3±0.7 12 36.678047 75.479797 1.3±0.2 13 36.798355 75.495140 4.6±0.9 14 36.851345 75.495140 4.6±0.9 15 36.955891 75.505592 2.7±0.7 16 36.878319 75.495140 4.6±0.9 17 36.939865 75.497597 4.2±0.7 18 36.966125 75.499939 2.6±0.5 19 36.497143 75.416504 1.1±0.3 20 36.5	137±1
4 36.706692 75.534019 2.2±0.1 5 36.824272 75.548027 3.1±0.2 6 36.721371 75.522621 2.3±0.2 7 36.851704 75.535210 2.9±0.3 8 36.815571 75.524368 4.4±0.9 9 36.968765 75.533386 2.4±0.6 10 36.673347 75.487823 2.5±0.8 11 36.630009 75.478310 2.3±0.7 12 36.678047 75.479797 1.3±0.2 13 36.798355 75.495140 4.6±0.9 14 36.851345 75.496162 2.8±0.7 15 36.955891 75.505592 2.7±0.7 16 36.878319 75.499311 2.9±0.2 17 36.939865 75.497597 4.2±0.7 18 36.966125 75.499939 2.6±0.5 19 36.497143 75.450340 1.8±0.3 21 36.792648 75.454046 1.7±0.3 22 36.	143±3
5 36.824272 75.548027 3.1±0.2 6 36.721371 75.522621 2.3±0.2 7 36.851704 75.535210 2.9±0.3 8 36.815571 75.524368 4.4±0.9 9 36.968765 75.533386 2.4±0.6 10 36.673347 75.487823 2.5±0.8 11 36.630009 75.478310 2.3±0.7 12 36.678047 75.479797 1.3±0.2 13 36.798355 75.495140 4.6±0.9 14 36.851345 75.496162 2.8±0.7 15 36.955891 75.505592 2.7±0.7 16 36.878319 75.489311 2.9±0.2 17 36.939865 75.497597 4.2±0.7 18 36.966125 75.499939 2.6±0.5 19 36.497143 75.416504 1.1±0.3 20 36.552902 75.420486 1.7±0.3 21 36.792648 75.4540453 2.2±0.4 22 3	124±5
6 36.721371 75.522621 2.3±0.2 7 36.851704 75.535210 2.9±0.3 8 36.815571 75.524368 4.4±0.9 9 36.968765 75.533386 2.4±0.6 10 36.673347 75.487823 2.5±0.8 11 36.630009 75.478310 2.3±0.7 12 36.678047 75.479797 1.3±0.2 13 36.798355 75.495140 4.6±0.9 14 36.851345 75.496162 2.8±0.7 15 36.955891 75.505592 2.7±0.7 16 36.878319 75.489311 2.9±0.2 17 36.939865 75.497597 4.2±0.7 18 36.966125 75.499939 2.6±0.5 19 36.497143 75.416504 1.1±0.3 20 36.552902 75.420486 1.7±0.3 21 36.792648 75.437553 3.4±0.5 22 36.801079 75.425781 3.5±0.5 23 3	129±2
7 36.851704 75.535210 2.9±0.3 8 36.815571 75.524368 4.4±0.9 9 36.968765 75.533386 2.4±0.6 10 36.673347 75.487823 2.5±0.8 11 36.630009 75.478310 2.3±0.7 12 36.678047 75.479797 1.3±0.2 13 36.798355 75.495140 4.6±0.9 14 36.851345 75.496162 2.8±0.7 15 36.955891 75.505592 2.7±0.7 16 36.878319 75.489311 2.9±0.2 17 36.939865 75.497597 4.2±0.7 18 36.966125 75.499939 2.6±0.5 19 36.497143 75.416504 1.1±0.3 20 36.552902 75.420486 1.7±0.3 21 36.792648 75.437553 3.4±0.5 22 36.801079 75.425781 3.5±0.5 24 36.688969 75.432584 3.0±0.4 25	105±2
8 36.815571 75.524368 4.4±0.9 9 36.968765 75.533386 2.4±0.6 10 36.673347 75.487823 2.5±0.8 11 36.630009 75.478310 2.3±0.7 12 36.678047 75.479797 1.3±0.2 13 36.798355 75.495140 4.6±0.9 14 36.851345 75.496162 2.8±0.7 15 36.955891 75.505592 2.7±0.7 16 36.878319 75.489311 2.9±0.2 17 36.939865 75.497597 4.2±0.7 18 36.966125 75.499939 2.6±0.5 19 36.497143 75.416504 1.1±0.3 20 36.552902 75.420486 1.7±0.3 21 36.792648 75.437553 3.4±0.5 24 36.881079 75.450340 1.8±0.3 23 36.717266 75.437553 3.4±0.5 24 36.688969 75.432884 3.0±0.4 25 36.536018 75.386826 5.4±1.6 28 36.536018	132±3
9 36.968765 75.533386 2.4±0.6 10 36.673347 75.487823 2.5±0.8 11 36.630009 75.478310 2.3±0.7 12 36.678047 75.479797 1.3±0.2 13 36.798355 75.495140 4.6±0.9 14 36.851345 75.496162 2.8±0.7 15 36.955891 75.505592 2.7±0.7 16 36.878319 75.489311 2.9±0.2 17 36.939865 75.497597 4.2±0.7 18 36.966125 75.499939 2.6±0.5 19 36.497143 75.416504 1.1±0.3 20 36.552902 75.420486 1.7±0.3 21 36.792648 75.454453 2.2±0.4 22 36.801079 75.450340 1.8±0.3 23 36.717266 75.437553 3.4±0.5 24 36.688969 75.432884 3.0±0.4 25 36.687901 75.425781 3.5±0.5 26 36.526684 75.392769 2.6±0.2 27 36.536018 75.386826 5.4±1.6 28 36.536018 75.386826 5.4±1.6 29 36.818443 75.420723 1.4±0.1 30 36.753849 75.409576 3.7±0.6 31 36.633022 75.388786 2.3±0.5 32 36.642246 75.385384 3.2±0.3 33 36.749104 75.400932 1.9±0.6 34 36.802547 75.408531 2.9±0.7 35 36.739025 75.388939 2.5±0.3 36.665897 75.374657 2.9±0.6 36.835003 75.38202 2.4±0.5 39 36.835003 75.38202 2.4±0.5 39 36.8441269 75.358467 1.9±0.2 40 36.828247 75.380699 2.8±0.2 41 36.441269 75.358467 1.9±0.2 42 36.642090 75.385460 2.5±0.6 43 36.464394 75.341240 2.6±0.3 44 36.718288 75.378220 1.5±0.5 45 36.507980 75.344017 2.0±0.6 46 36.482780 75.326973 2.8±0.6 47 36.543869 75.321381 1.4±0.4 48 36.667274 75.338501 1.6±0.1	129±3
10 36.673347 75.487823 2.5±0.8 11 36.630009 75.478310 2.3±0.7 12 36.678047 75.479797 1.3±0.2 13 36.798355 75.495140 4.6±0.9 14 36.851345 75.496162 2.8±0.7 15 36.955891 75.505592 2.7±0.7 16 36.878319 75.489311 2.9±0.2 17 36.939865 75.497597 4.2±0.7 18 36.966125 75.499939 2.6±0.5 19 36.497143 75.416504 1.1±0.3 20 36.552902 75.420486 1.7±0.3 21 36.792648 75.4544453 2.2±0.4 22 36.801079 75.450340 1.8±0.3 23 36.717266 75.437553 3.4±0.5 24 36.688969 75.425781 3.5±0.5 25 36.536018 75.386826 5.4±1.6 28 36.536018 75.386826 5.4±1.6 29	124±6
11 36.630009 75.478310 2.3±0.7 12 36.678047 75.479797 1.3±0.2 13 36.798355 75.495140 4.6±0.9 14 36.851345 75.496162 2.8±0.7 15 36.955891 75.505592 2.7±0.7 16 36.878319 75.489311 2.9±0.2 17 36.939865 75.497597 4.2±0.7 18 36.966125 75.499939 2.6±0.5 19 36.497143 75.416504 1.1±0.3 20 36.552902 75.420486 1.7±0.3 21 36.792648 75.4544453 2.2±0.4 22 36.801079 75.450340 1.8±0.3 23 36.717266 75.437553 3.4±0.5 24 36.688969 75.432884 3.0±0.4 25 36.687901 75.425781 3.5±0.5 26 36.536018 75.386826 5.4±1.6 28 36.536018 75.386826 5.4±1.6 29	120±7
12 36.678047 75.479797 1.3±0.2 13 36.798355 75.495140 4.6±0.9 14 36.851345 75.496162 2.8±0.7 15 36.955891 75.505592 2.7±0.7 16 36.878319 75.489311 2.9±0.2 17 36.939865 75.497597 4.2±0.7 18 36.966125 75.499939 2.6±0.5 19 36.497143 75.416504 1.1±0.3 20 36.552902 75.420486 1.7±0.3 21 36.792648 75.4544453 2.2±0.4 22 36.801079 75.450340 1.8±0.3 23 36.717266 75.437553 3.4±0.5 24 36.688969 75.425781 3.5±0.5 25 36.687901 75.425781 3.5±0.5 26 36.526684 75.392769 2.6±0.2 27 36.536018 75.386826 5.4±1.6 28 36.536018 75.386826 5.4±1.6 29	123±8
13 36.798355 75.495140 4.6±0.9 14 36.851345 75.496162 2.8±0.7 15 36.955891 75.505592 2.7±0.7 16 36.878319 75.489311 2.9±0.2 17 36.939865 75.497597 4.2±0.7 18 36.966125 75.499939 2.6±0.5 19 36.497143 75.416504 1.1±0.3 20 36.552902 75.420486 1.7±0.3 21 36.792648 75.4544453 2.2±0.4 22 36.801079 75.450340 1.8±0.3 23 36.717266 75.437553 3.4±0.5 24 36.688969 75.425781 3.5±0.5 25 36.536018 75.386826 5.4±1.6 28 36.536018 75.386826 5.4±1.6 29 36.818443 75.409576 3.7±0.6 31 36.633022 75.388786 2.3±0.5 32 36.642246 75.385384 3.2±0.3 33	132±8
14 36.851345 75.496162 2.8±0.7 15 36.955891 75.505592 2.7±0.7 16 36.878319 75.489311 2.9±0.2 17 36.939865 75.497597 4.2±0.7 18 36.966125 75.499939 2.6±0.5 19 36.497143 75.416504 1.1±0.3 20 36.552902 75.420486 1.7±0.3 21 36.792648 75.454453 2.2±0.4 22 36.801079 75.450340 1.8±0.3 23 36.717266 75.437553 3.4±0.5 24 36.688969 75.432884 3.0±0.4 25 36.536018 75.386826 5.4±1.6 28 36.536018 75.386826 5.4±1.6 29 36.818443 75.409576 3.7±0.6 31 36.633022 75.388786 2.3±0.5 32 36.642246 75.385384 3.2±0.3 33 36.749104 75.409531 2.9±0.7 35 <	120±5
15 36.955891 75.505592 2.7±0.7 16 36.878319 75.489311 2.9±0.2 17 36.939865 75.497597 4.2±0.7 18 36.966125 75.499939 2.6±0.5 19 36.497143 75.416504 1.1±0.3 20 36.552902 75.420486 1.7±0.3 21 36.792648 75.450340 1.8±0.3 22 36.801079 75.450340 1.8±0.3 23 36.717266 75.437553 3.4±0.5 24 36.688969 75.425781 3.5±0.5 24 36.526684 75.392769 2.6±0.2 27 36.536018 75.386826 5.4±1.6 28 36.536018 75.386826 5.4±1.6 29 36.818443 75.409576 3.7±0.6 31 36.633022 75.388786 2.3±0.5 32 36.642246 75.385384 3.2±0.3 33 36.749104 75.408531 2.9±0.7 35 <	123±6
16 36.878319 75.489311 2.9±0.2 17 36.939865 75.497597 4.2±0.7 18 36.966125 75.499939 2.6±0.5 19 36.497143 75.416504 1.1±0.3 20 36.552902 75.420486 1.7±0.3 21 36.792648 75.450340 1.8±0.3 21 36.801079 75.450340 1.8±0.3 23 36.717266 75.437553 3.4±0.5 24 36.688969 75.432884 3.0±0.4 25 36.687901 75.425781 3.5±0.5 26 36.526684 75.392769 2.6±0.2 27 36.536018 75.386826 5.4±1.6 28 36.536018 75.386826 5.4±1.6 29 36.818443 75.409576 3.7±0.6 31 36.633022 75.388786 2.3±0.5 32 36.642246 75.385384 3.2±0.3 33 36.749104 75.409531 2.9±0.7 35 <	119±7
17 36.939865 75.497597 4.2±0.7 18 36.966125 75.499939 2.6±0.5 19 36.497143 75.416504 1.1±0.3 20 36.552902 75.420486 1.7±0.3 21 36.792648 75.450340 1.8±0.3 22 36.801079 75.450340 1.8±0.3 23 36.717266 75.437553 3.4±0.5 24 36.688969 75.432884 3.0±0.4 25 36.687901 75.425781 3.5±0.5 26 36.526684 75.392769 2.6±0.2 27 36.536018 75.386826 5.4±1.6 28 36.536018 75.386826 5.4±1.6 29 36.818443 75.409576 3.7±0.6 31 36.633022 75.388786 2.3±0.5 32 36.642246 75.385384 3.2±0.3 33 36.749104 75.409576 3.7±0.6 34 36.802547 75.408531 2.9±0.7 35 <	110±7 124±2
18 36.966125 75.499939 2.6±0.5 19 36.497143 75.416504 1.1±0.3 20 36.552902 75.420486 1.7±0.3 21 36.792648 75.450340 1.8±0.3 22 36.801079 75.450340 1.8±0.3 23 36.717266 75.437553 3.4±0.5 24 36.688969 75.432884 3.0±0.4 25 36.687901 75.425781 3.5±0.5 26 36.526684 75.392769 2.6±0.2 27 36.536018 75.386826 5.4±1.6 28 36.536018 75.386826 5.4±1.6 29 36.818443 75.420723 1.4±0.1 30 36.753849 75.409576 3.7±0.6 31 36.633022 75.388786 2.3±0.5 32 36.642246 75.385384 3.2±0.3 33 36.749104 75.400932 1.9±0.6 34 36.802547 75.408531 2.9±0.7 35 <	124±2 115±4
19 36.497143 75.416504 1.1±0.3 20 36.552902 75.420486 1.7±0.3 21 36.792648 75.4504453 2.2±0.4 22 36.801079 75.450340 1.8±0.3 23 36.717266 75.437553 3.4±0.5 24 36.688969 75.432884 3.0±0.4 25 36.687901 75.425781 3.5±0.5 26 36.526684 75.392769 2.6±0.2 27 36.536018 75.386826 5.4±1.6 28 36.536018 75.386826 5.4±1.6 29 36.818443 75.420723 1.4±0.1 30 36.753849 75.409576 3.7±0.6 31 36.633022 75.388786 2.3±0.5 32 36.642246 75.385384 3.2±0.3 33 36.749104 75.408531 2.9±0.7 34 36.802547 75.408531 2.9±0.7 35 36.739025 75.388939 2.5±0.3 36	113±4 124±5
20 36.552902 75.420486 1.7±0.3 21 36.792648 75.4544453 2.2±0.4 22 36.801079 75.450340 1.8±0.3 23 36.717266 75.437553 3.4±0.5 24 36.688969 75.432884 3.0±0.4 25 36.687901 75.425781 3.5±0.5 26 36.526684 75.392769 2.6±0.2 27 36.536018 75.386826 5.4±1.6 28 36.536018 75.386826 5.4±1.6 29 36.818443 75.420723 1.4±0.1 30 36.753849 75.409576 3.7±0.6 31 36.633022 75.388786 2.3±0.5 32 36.642246 75.385384 3.2±0.3 33 36.749104 75.409531 2.9±0.7 35 36.739025 75.388939 2.5±0.3 36 36.682495 75.374657 2.9±0.6 38 36.816051 75.384026 2.9±0.1 39	89±7
21 36.792648 75.454453 2.2±0.4 22 36.801079 75.450340 1.8±0.3 23 36.717266 75.437553 3.4±0.5 24 36.688969 75.432884 3.0±0.4 25 36.687901 75.425781 3.5±0.5 26 36.526684 75.392769 2.6±0.2 27 36.536018 75.386826 5.4±1.6 28 36.536018 75.386826 5.4±1.6 29 36.818443 75.420723 1.4±0.1 30 36.753849 75.409576 3.7±0.6 31 36.633022 75.388786 2.3±0.5 32 36.642246 75.385384 3.2±0.3 33 36.749104 75.400932 1.9±0.6 34 36.802547 75.408531 2.9±0.7 35 36.739025 75.388939 2.5±0.3 36 36.6582495 75.374657 2.9±0.6 38 36.816051 75.384026 2.9±0.1 39	115±5
22 36.801079 75.450340 1.8±0.3 23 36.717266 75.437553 3.4±0.5 24 36.688969 75.432884 3.0±0.4 25 36.687901 75.425781 3.5±0.5 26 36.526684 75.392769 2.6±0.2 27 36.536018 75.386826 5.4±1.6 28 36.536018 75.386826 5.4±1.6 29 36.818443 75.420723 1.4±0.1 30 36.753849 75.409576 3.7±0.6 31 36.633022 75.388786 2.3±0.5 32 36.642246 75.385384 3.2±0.3 33 36.749104 75.400932 1.9±0.6 34 36.802547 75.408531 2.9±0.7 35 36.739025 75.388939 2.5±0.3 36 36.682495 75.374657 2.9±0.6 38 36.816051 75.384026 2.9±0.1 39 36.835003 75.382202 2.4±0.5 40 <	119±5
23 36.717266 75.437553 3.4±0.5 24 36.688969 75.432884 3.0±0.4 25 36.687901 75.425781 3.5±0.5 26 36.526684 75.392769 2.6±0.2 27 36.536018 75.386826 5.4±1.6 28 36.536018 75.386826 5.4±1.6 29 36.818443 75.420723 1.4±0.1 30 36.753849 75.409576 3.7±0.6 31 36.633022 75.388786 2.3±0.5 32 36.642246 75.385384 3.2±0.3 33 36.749104 75.400932 1.9±0.6 34 36.802547 75.408531 2.9±0.7 35 36.739025 75.388939 2.5±0.3 36 36.682495 75.374657 2.9±0.6 38 36.816051 75.384026 2.9±0.1 39 36.835003 75.382202 2.4±0.5 40 36.828247 75.380699 2.8±0.2 41 <	105±5
24 36.688969 75.432884 3.0±0.4 25 36.687901 75.425781 3.5±0.5 26 36.526684 75.392769 2.6±0.2 27 36.536018 75.386826 5.4±1.6 28 36.536018 75.386826 5.4±1.6 29 36.818443 75.420723 1.4±0.1 30 36.753849 75.409576 3.7±0.6 31 36.633022 75.388786 2.3±0.5 32 36.642246 75.385384 3.2±0.3 33 36.749104 75.400932 1.9±0.6 34 36.802547 75.408531 2.9±0.7 35 36.739025 75.388939 2.5±0.3 36 36.682495 75.379448 2.4±0.5 37 36.665897 75.374657 2.9±0.6 38 36.816051 75.384026 2.9±0.1 39 36.828247 75.380699 2.8±0.2 41 36.441269 75.358467 1.9±0.2 42 <	129±4
25 36.687901 75.425781 3.5±0.5 26 36.526684 75.392769 2.6±0.2 27 36.536018 75.386826 5.4±1.6 28 36.536018 75.386826 5.4±1.6 29 36.818443 75.420723 1.4±0.1 30 36.753849 75.409576 3.7±0.6 31 36.633022 75.388786 2.3±0.5 32 36.642246 75.385384 3.2±0.3 33 36.749104 75.400932 1.9±0.6 34 36.802547 75.408531 2.9±0.7 35 36.739025 75.388939 2.5±0.3 36 36.682495 75.379448 2.4±0.5 37 36.665897 75.374657 2.9±0.6 38 36.816051 75.384026 2.9±0.1 39 36.835003 75.382202 2.4±0.5 40 36.828247 75.380699 2.8±0.2 41 36.441269 75.358467 1.9±0.2 42 <	121±3
26 36.526684 75.392769 2.6±0.2 27 36.536018 75.386826 5.4±1.6 28 36.536018 75.386826 5.4±1.6 29 36.818443 75.420723 1.4±0.1 30 36.753849 75.409576 3.7±0.6 31 36.633022 75.388786 2.3±0.5 32 36.642246 75.385384 3.2±0.3 33 36.749104 75.400932 1.9±0.6 34 36.802547 75.408531 2.9±0.7 35 36.739025 75.388939 2.5±0.3 36 36.682495 75.379448 2.4±0.5 37 36.665897 75.374657 2.9±0.6 38 36.816051 75.384026 2.9±0.1 39 36.835003 75.382202 2.4±0.5 40 36.828247 75.380699 2.8±0.2 41 36.441269 75.385460 2.5±0.6 43 36.464394 75.341240 2.6±0.3 44 <	135±4
27 36.536018 75.386826 5.4±1.6 28 36.536018 75.386826 5.4±1.6 29 36.818443 75.420723 1.4±0.1 30 36.753849 75.409576 3.7±0.6 31 36.633022 75.388786 2.3±0.5 32 36.642246 75.385384 3.2±0.3 33 36.749104 75.400932 1.9±0.6 34 36.802547 75.408531 2.9±0.7 35 36.739025 75.388939 2.5±0.3 36 36.682495 75.379448 2.4±0.5 37 36.665897 75.374657 2.9±0.6 38 36.816051 75.384026 2.9±0.1 39 36.828247 75.380699 2.8±0.2 41 36.441269 75.358467 1.9±0.2 42 36.642090 75.385460 2.5±0.6 43 36.464394 75.341240 2.6±0.3 44 36.718288 75.378220 1.5±0.5 45 <	128±2
28 36.536018 75.386826 5.4±1.6 29 36.818443 75.420723 1.4±0.1 30 36.753849 75.409576 3.7±0.6 31 36.633022 75.388786 2.3±0.5 32 36.642246 75.385384 3.2±0.3 33 36.749104 75.400932 1.9±0.6 34 36.802547 75.408531 2.9±0.7 35 36.739025 75.388939 2.5±0.3 36 36.682495 75.379448 2.4±0.5 37 36.665897 75.374657 2.9±0.6 38 36.816051 75.384026 2.9±0.1 39 36.835003 75.382202 2.4±0.5 40 36.828247 75.380699 2.8±0.2 41 36.441269 75.358467 1.9±0.2 42 36.642090 75.385460 2.5±0.6 43 36.718288 75.378220 1.5±0.5 45 36.507980 75.344017 2.0±0.6 45 <	86±8
29 36.818443 75.420723 1.4±0.1 30 36.753849 75.409576 3.7±0.6 31 36.633022 75.388786 2.3±0.5 32 36.642246 75.385384 3.2±0.3 33 36.749104 75.400932 1.9±0.6 34 36.802547 75.408531 2.9±0.7 35 36.739025 75.388939 2.5±0.3 36 36.682495 75.379448 2.4±0.5 37 36.665897 75.374657 2.9±0.6 38 36.816051 75.384026 2.9±0.1 39 36.835003 75.382202 2.4±0.5 40 36.828247 75.380699 2.8±0.2 41 36.441269 75.385467 1.9±0.2 42 36.642090 75.385460 2.5±0.6 43 36.464394 75.341240 2.6±0.3 44 36.718288 75.378220 1.5±0.5 45 36.507980 75.344017 2.0±0.6 46 <	86±8
30 36.753849 75.409576 3.7±0.6 31 36.633022 75.388786 2.3±0.5 32 36.642246 75.385384 3.2±0.3 33 36.749104 75.400932 1.9±0.6 34 36.802547 75.408531 2.9±0.7 35 36.739025 75.388939 2.5±0.3 36 36.682495 75.379448 2.4±0.5 37 36.665897 75.374657 2.9±0.6 38 36.816051 75.384026 2.9±0.1 39 36.835003 75.382202 2.4±0.5 40 36.828247 75.380699 2.8±0.2 41 36.441269 75.358467 1.9±0.2 42 36.642090 75.385460 2.5±0.6 43 36.718288 75.378220 1.5±0.5 45 36.507980 75.344017 2.0±0.6 46 36.482780 75.326973 2.8±0.6 47 36.543869 75.321381 1.4±0.4 48 <	102±3
31 36.633022 75.388786 2.3±0.5 32 36.642246 75.385384 3.2±0.3 33 36.749104 75.400932 1.9±0.6 34 36.802547 75.408531 2.9±0.7 35 36.739025 75.388939 2.5±0.3 36 36.682495 75.379448 2.4±0.5 37 36.665897 75.374657 2.9±0.6 38 36.816051 75.384026 2.9±0.1 39 36.835003 75.382202 2.4±0.5 40 36.828247 75.380699 2.8±0.2 41 36.441269 75.358467 1.9±0.2 42 36.642090 75.385460 2.5±0.6 43 36.464394 75.341240 2.6±0.3 44 36.718288 75.378220 1.5±0.5 45 36.507980 75.344017 2.0±0.6 46 36.482780 75.326973 2.8±0.6 47 36.543869 75.321381 1.4±0.4 48 <	120±4
$\begin{array}{cccccccccccccccccccccccccccccccccccc$	124±6
$\begin{array}{cccccccccccccccccccccccccccccccccccc$	140±3
35 36.739025 75.388939 2.5±0.3 36 36.682495 75.379448 2.4±0.5 37 36.665897 75.374657 2.9±0.6 38 36.816051 75.384026 2.9±0.1 39 36.835003 75.382202 2.4±0.5 40 36.828247 75.380699 2.8±0.2 41 36.441269 75.358467 1.9±0.2 42 36.642090 75.385460 2.5±0.6 43 36.464394 75.341240 2.6±0.3 44 36.718288 75.378220 1.5±0.5 45 36.507980 75.344017 2.0±0.6 46 36.482780 75.326973 2.8±0.6 47 36.543869 75.321381 1.4±0.4 48 36.667274 75.338501 1.6±0.1	111±9
36 36.682495 75.379448 2.4±0.5 37 36.665897 75.374657 2.9±0.6 38 36.816051 75.384026 2.9±0.1 39 36.835003 75.382202 2.4±0.5 40 36.828247 75.380699 2.8±0.2 41 36.441269 75.358467 1.9±0.2 42 36.642090 75.385460 2.5±0.6 43 36.464394 75.341240 2.6±0.3 44 36.718288 75.378220 1.5±0.5 45 36.507980 75.344017 2.0±0.6 46 36.482780 75.326973 2.8±0.6 47 36.543869 75.321381 1.4±0.4 48 36.667274 75.338501 1.6±0.1	122±7
$\begin{array}{cccccccccccccccccccccccccccccccccccc$	126±4
38 36.816051 75.384026 2.9±0.1 39 36.835003 75.382202 2.4±0.5 40 36.828247 75.380699 2.8±0.2 41 36.441269 75.358467 1.9±0.2 42 36.642090 75.385460 2.5±0.6 43 36.464394 75.341240 2.6±0.3 44 36.718288 75.378220 1.5±0.5 45 36.507980 75.344017 2.0±0.6 46 36.482780 75.326973 2.8±0.6 47 36.543869 75.321381 1.4±0.4 48 36.667274 75.338501 1.6±0.1	137±6
39 36.835003 75.382202 2.4±0.5 40 36.828247 75.380699 2.8±0.2 41 36.441269 75.358467 1.9±0.2 42 36.642090 75.385460 2.5±0.6 43 36.464394 75.341240 2.6±0.3 44 36.718288 75.378220 1.5±0.5 45 36.507980 75.344017 2.0±0.6 46 36.482780 75.326973 2.8±0.6 47 36.543869 75.321381 1.4±0.4 48 36.667274 75.338501 1.6±0.1	138±6
$\begin{array}{cccccccccccccccccccccccccccccccccccc$	131±1
$\begin{array}{cccccccccccccccccccccccccccccccccccc$	143±5
$\begin{array}{cccccccccccccccccccccccccccccccccccc$	143 ± 2
$\begin{array}{cccccccccccccccccccccccccccccccccccc$	143 ± 2
$\begin{array}{cccccccccccccccccccccccccccccccccccc$	136±6
$\begin{array}{cccccccccccccccccccccccccccccccccccc$	141±3
46 36.482780 75.326973 2.8±0.6 47 36.543869 75.321381 1.4±0.4 48 36.667274 75.338501 1.6±0.1	136±9
47 36.543869 75.321381 1.4±0.4 48 36.667274 75.338501 1.6±0.1	150±9
$48 \qquad 36.667274 \qquad 75.338501 \qquad 1.6 {\pm} 0.1$	178±5
	99±8
4U 36.640007 75.224670 2.2.0.4	120±2
	144±3
50 36.810066 75.356255 2.3±0.3	131±4
51 36.708378 75.339081 5.7±0.8	120±4
52 36.821564 75.353394 3.4±0.7	140±6
53 36.804974 75.349754 1.9 ± 0.6	118±8
54 36.869255 75.347252 6.7±0.6	100±3
55 36.892963 75.334496 1.7±0.5 56 36.733772 75.309822 2.8±0.8	90±8 103±8

57 36.704391 75.294312 2.4 ± 0.7 135 ± 8 58 2.1 ± 0.4 36.889622 75.319733 134 ± 5 59 3.6 ± 0.4 36.900982 75.320618 120 ± 3 60 36.840511 75.308975 3.2 ± 0.5 125 ± 5 36.778320 75.293205 1.9 ± 0.2 123 ± 3 61 62 36.760612 75.289764 2.2 ± 0.5 125±6 63 75.280144 2.4 ± 0.4 36.718964 138±5 64 36.160011 75.387260 1.9 ± 0.6 2 ± 8 65 36.042805 75.369087 1.6 ± 0.3 108 ± 5 66 36.107712 75.358253 1.1 ± 0.3 111±8 0.9 ± 0.2 67 36.175201 75.364693 107 ± 7 1.6 ± 0.3 68 36.222542 75.360321 93±5 69 36.237003 75.340622 3.2 ± 0.6 97±5 70 36.180279 75.328026 5.4 ± 0.8 138±4 71 36.326046 75.343208 1.7 ± 0.1 131±2 72 36.036568 75.296249 0.8 ± 0.1 118±5 73 36.382717 75.343605 0.6 ± 0.1 132 ± 4 74 36.175095 75.304520 2.0 ± 0.6 137±8 75 36.115463 75.294716 2.9 ± 0.7 91±7 76 36.272186 75.297707 1.4 ± 0.3 110±6 77 36.343594 75.301308 8.6 ± 0.8 129±3 78 36.249485 75.279053 2.0 ± 0.5 112±6 79 35.723125 75.319908 4.4 ± 0.7 17±5 80 35.775055 75.311264 3.4 ± 0.7 113 ± 6 81 35.802952 75.313507 3.8 ± 0.7 42±5 82 36.107559 75.358276 1.7 ± 0.3 100 ± 5 83 35.847786 75.315231 2.8 ± 0.6 104±6 84 36.175217 75.364716 0.9 ± 0.2 122±6 85 36.172031 75.356987 0.8 ± 0.2 87±7 35.977787 75.291695 1.1 ± 0.2 86 120±5 87 36.036797 75.296349 1.1 ± 0.2 118±5 88 2.5 ± 0.3 35.719463 75.561485 110±4 89 35.877468 75.583862 3.2 ± 0.5 120±4 90 35.790482 75.547256 7.0 ± 0.8 95±3 91 35.805134 75.541405 5.3 ± 0.5 113±3 92 36.025848 75.573044 3.9 ± 0.3 127±2 93 3.2 ± 0.2 36.011715 75.570824 111±2 94 35.886318 75.550804 3.6 ± 0.2 125 ± 1 95 35.829212 75.532265 3.7 ± 0.1 111±1 96 36.057571 75.566589 3.4 ± 0.2 122 ± 2 97 35.937981 75.543114 6.1 ± 0.7 113 ± 3 98 4.2 ± 0.5 121±3 36.150185 75.572212 99 3.0 ± 0.1 35.846653 75.511169 122 ± 1 100 35.839558 75.508217 2.8 ± 0.4 110 ± 4 101 36.047020 75.528419 3.5 ± 0.7 134 ± 5 102 35.937199 75.511421 3.2 ± 0.3 113 ± 2 103 75.514542 36.000168 3.3 ± 0.7 118±6 104 75.528450 4.7 ± 1.2 36.131355 106±7 105 35.902927 75.491394 1.7 ± 0.3 115±5 106 36.158512 75.521553 6.6 ± 0.7 109±3 107 35.964561 75.486557 1.7 ± 0.3 117±5 108 36.240715 75.615578 3.6 ± 1.1 105±9 109 36.288883 75.621521 5.4 ± 0.4 106±2 110 36.342354 75.613274 3.6 ± 0.2 115±2 36.307533 75.579750 7.6 ± 1.4 111 123±5 112 36.302315 75.571709 3.6 ± 1.2 93±9 3.2 ± 0.2 124 ± 2 113 36.300140 75.569557 114 36.273445 75.537132 5.3 ± 1.2 116±6 115 36.435184 75.543159 3.3 ± 0.8 118±7 36.651173 75.574608 4.5 ± 0.5 116 171±3

117	35.726604	75.429031	1.9±0.5	106±6	41	67.476395	26.272152	3.7±0.3
118	35.770763	75.471237	1.4±0.3	121±16	42	67.480774	26.266171	3.0±0.5
119	35.806629	75.463112	2.8±0.4	110±5	43	67.455139	26.249735	3.9±0.
120	35.798588	75.452263	7.5±1.1	10±3 101±4	44	67.527328	26.288523	4.2±0.
			7.3 ± 1.1 2.4 ± 0.4		45			
121	35.877754	75.488167		146±5		67.528503	26.285934	4.1±0.
122	35.829231	75.408340	1.8±0.6	145±8	46	67.448624	26.232401	3.0±0.
123	35.863377	75.437630	2.1 ± 0.6	167 ± 2	47	67.518898	26.267067	$3.3\pm0.$
124	35.860695	75.387650	4.0 ± 0.4	8±3	48	67.552650	26.275578	$2.8 \pm 0.$
125	35.980408	75.409248	1.5 ± 0.3	109±9	49	67.447762	26.217007	$3.8 \pm 1.$
126	36.039444	75.484955	4.0 ± 1.3	8±8	50	67.466057	26.223522	$3.9 \pm 0.$
127	36.241055	75.463737	4.2 ± 0.7	124 ± 5	51	67.464447	26.207251	$3.6\pm0.$
128	36.269241	75.474220	5.0 ± 0.7	126±4	52	67.528458	26.232956	$3.8 \pm 0.$
129	36.302826	75.503593	3.4 ± 0.4	122±4	53	67.519531	26.227768	3.3±0.
130	36.282207	75.472626	2.6±0.5	118±5	54	67.484222	26.207764	3.9±0.
131	36.319000	75.460953	4.0±0.6	136±4	55	67.501228	26.207205	3.1±0.
132	36.392452	75.496414	7.8 ± 0.5	108±2	56	67.559822	26.236757	$2.7\pm0.$
133	36.402100	75.469627	3.4±0.3	114±3	57	67.527458	26.214884	2.9±0.
134	36.399605	75.445602	2.5±0.4	109±5	58	67.157364	26.257944	2.3±0.
135	36.437878	75.444946	2.7 ± 0.3	131±3	59	67.167305	26.259041	$3.5\pm0.$
		I 1501E			- 60	67.188629	26.257345	$2.3\pm0.$
		L1521E			61	67.238670	26.277580	$2.1\pm0.$
1	67.481590	26.287052	4.6±0.4	26±2	62	67.176338	26.236416	$2.0\pm0.$
2	67.476410	26.272148	5.0±0.9	24±5	63	67.257874	26.266144	$6.0\pm1.$
3	67.527367	26.288368	4.2±0.3	22±2	64	67.263107	26.268164	2.7±0.
4	67.528519	26.285912	4.2±0.3 4.3±0.3	26±2	65	67.256348	26.263693	2.8±0.
5					66	67.255142	26.262440	2.7±0.
	67.560616	26.291574	3.0 ± 0.2	30±2	67	67.212830	26.238308	2.1±0.
6	67.518944	26.267017	3.2±0.2	26±1				
7	67.552635	26.275476	3.6 ± 0.4	24±3	68	67.188499	26.224091	2.3±0.
8	67.519592	26.227743	2.9 ± 0.5	29 ± 5	69	67.203880	26.230350	2.4±0.
9	67.542175	26.225372	4.0 ± 0.1	20 ± 1	70	67.200729	26.221565	2.3±0.
10	67.598625	26.241295	3.0 ± 0.2	23 ± 1	71	67.218590	26.212732	6.1±1.
11	67.580704	26.221781	3.4 ± 0.4	14±4	72	67.229462	26.203793	$2.8\pm0.$
12	67.352890	26.136698	1.8 ± 0.4	38±5	73	67.259682	26.213427	$4.1\pm1.$
13	67.339035	26.116142	1.8 ± 0.4	27±6	74	67.379425	26.458372	$3.5 \pm 0.$
14	67.349022	26.116617	2.7 ± 0.7	35±7	75	67.352814	26.426369	$3.0\pm0.$
15	67.369499	26.120598	2.1±0.1	32±2	76	67.417671	26.460176	2.9±0.
16	67.389580	26.127825	3.1 ± 0.5	26±5	77	67.375343	26.433187	3.2±0.
17	67.426331	26.144903	2.6 ± 0.0	20±3 27±1	78	67.372414	26.429434	3.0±0.
18					79	67.372414	26.429434	3.0±0.
	67.335449	26.083839	2.2±0.6	48±8	80	67.375771	26.414431	3.3±0.
19	67.379005	26.107500	3.6 ± 0.6	28±5	81	67.370667	26.387484	3.0±0.
20	67.403671	26.115255	2.1±0.2	29±3				
21	67.354576	26.085054	2.6 ± 0.8	29±8	82	67.449181	26.426167	3.5±0.
22	67.388283	26.098785	2.3 ± 0.6	21±8	83	67.436790	26.414555	3.3±0.
23	67.440826	26.127062	3.1 ± 0.9	36±7	84	67.453255	26.422728	2.9±0.
24	67.358475	26.080219	2.1 ± 0.1	33 ± 1	85	67.453255	26.422728	$2.9\pm0.$
25	67.447426	26.117859	4.1 ± 0.4	25±3	86	67.447006	26.415834	$3.7\pm0.$
26	67.430061	26.104013	2.5 ± 0.2	29±2	87	67.454948	26.414957	$6.0 \pm 1.$
27	67.462196	26.114037	3.7 ± 0.4	31±3	88	67.396027	26.382881	$4.0\pm0.$
28	67.464890	26.112408	2.8±0.1	45±1	89	67.404182	26.366709	2.5±0.
29	67.447563	26.098097	2.3 ± 0.1 2.3 ± 0.2	33±3	90	67.423317	26.372372	4.5±0.
					91	67.438324	26.377171	3.1±0.
30	67.373581	26.056162	2.8 ± 0.7	45±7	92	67.429680	26.369631	4.0±0.
31	67.410774	26.075914	1.6±0.5	36±7	92			
32	67.412727	26.072020	3.1±0.7	24±6		67.319107	26.209984	$2.0\pm0.$
33	67.435532	26.075167	3.1 ± 0.5	35 ± 5	94	67.296135	26.196365	2.7±0.
34	67.408218	26.056572	2.9 ± 0.2	32 ± 2	95	67.318672	26.163237	1.7±0.
35	67.403999	26.050295	3.0 ± 0.4	31±3	96	67.311264	26.158535	$2.0\pm0.$
36	67.373482	26.152620	1.9 ± 0.1	35 ± 1	97	67.324203	26.163578	$2.3\pm0.$
37	67.458282	26.297251	3.3±0.6	30±5	98	67.369453	26.120644	$2.2 \pm 0.$
38	67.468719	26.287107	3.8±0.2	32±1				
39	67.481529	26.287107	3.9 ± 0.2	34±2				
40								
40	67.455322	26.271738	3.3 ± 0.2	34±1				

		L1517		
		L1517		
1	73.722855	30.501905	3.3 ± 0.9	97±8
2	73.714233	30.483135	4.0 ± 0.6	74±4
3	73.722137	30.477777	5.8 ± 0.8	77±4
4	73.770859	30.500072	1.3 ± 0.4	78±9
5	73.769554	30.497047	3.5 ± 0.2	78 ± 2
6	73.719040	30.469999	1.8 ± 0.3	90 ± 5
7	73.696213	30.443743	6.3 ± 0.5	106±2
8	73.779846	30.482695	2.3 ± 0.2	51±3
9	73.730705	30.456091	1.4 ± 0.3	75±6
10	73.750389	30.461250	1.8 ± 0.3	73±6
11	73.733681	30.446335	7.2 ± 2.2	116±8
12	73.741402	30.446253	1.9 ± 0.4	191±7
13	73.755302	30.450823	1.0 ± 0.2	84±7
14	73.740608	30.436319	2.3 ± 0.2	197±3
15	73.781036	30.456249	1.4 ± 0.5	82±10
16	73.761192	30.445122	4.2 ± 0.4	94±3
17	73.736732	30.426329	1.1±0.1	159±2
18	73.733017	30.424347	3.1 ± 1.0	186±9
19	73.814430	30.450090	4.8±0.7	34±4
20	73.779900	30.482515	3.2±0.4	91±4
21	73.821487	30.502167	2.0±0.3	47±5
22	73.825714	30.500570	1.8±0.2	54±4
23	73.847931	30.506588	1.5±0.4	47±8
24	73.863907	30.510509	1.7±0.4	52±7
25	73.849792	30.493942	1.5±0.4	79±7
26	73.781036	30.456135	2.1±0.5	74±6
27	73.883133	30.506731	2.2±0.5	82±6
28	73.811386	30.466928	5.7±1.1	197±5
29	73.882698	30.500095	2.6±0.1	66±1
30	73.832230	30.462818	1.6±0.3	74±6
31	73.788635	30.439535	1.6±0.4	53±6
32	73.904160	30.487429	3.9±0.9	86±7
33	73.847229	30.445190	2.8 ± 0.6	78±6
34	73.797928	30.416260	4.8±0.7	46±4
35	73.802299	30.418278	1.6±0.7	75±6
36	73.916710	30.468847	1.1±0.1	96±3
37	73.823593	30.422194	2.0 ± 0.7	91±9
38	73.908470	30.463478	0.6 ± 0.2	88±7
39	73.825531	30.417072	3.0±0.9	85±9
40	73.889534	30.445328	1.6±0.4	133±7
41	73.905228	30.427259	2.7±0.1	111±1
42	73.881660	30.644161	2.5 ± 0.4	58±4
43	73.858200	30.594833	2.7 ± 0.7	84±7
44	73.866859	30.585754	2.7 ± 0.7 2.7 ± 0.3	79±3
45	73.897896	30.596272	2.1±0.5	80±7
46	73.903664	30.592806	1.6±0.3	73±5
47	73.909607	30.590330	2.2±0.3	96±4
48	73.913071	30.583788	2.2±0.3 2.2±0.4	91±5
49	73.865555	30.558216	3.0 ± 0.3	63±3
50	73.865150	30.556414	2.2±0.1	73±2
51	73.885841	30.644678	1.1 ± 0.2	81±6
52	73.897606	30.577805	1.8±0.1	81±0
53	73.945488	30.538900	5.3 ± 0.7	94±4
54	73.945488	30.538900	3.3±0.7 2.8±0.7	94±4 71±7
55	73.943163	30.527084	2.8±0.7 1.5±0.3	70±6
56	74.040062	30.525234	2.1±0.6	103±8
57 59	73.917236	30.493732	1.6 ± 0.1	64±25
58	73.980095	30.511055	3.7 ± 0.9	96±7
59	73.942177	30.491476	7.4 ± 0.4	86±5

20	76.101997	32.863926	1.4 ± 0.1	189±2	80	76.134727	32.752444	2.8 ± 0.4	198±4
21	76.117981	32.911945	1.1 ± 0.3	178±7	81	76.147842	32.793490	1.8 ± 0.6	101±10
22	76.126297	32.907944	1.5 ± 0.1	165±2	82	76.162682	32.800082	6.1 ± 0.3	98±1
23	76.153435	32.867275	2.7 ± 0.8	158±9	83	76.160995	32.789722	2.9 ± 0.3	137±3
24	76.171211	32.901875	2.7 ± 0.3	171±3	84	76.160347	32.760299	3.1 ± 0.2	116±4
25	76.179031	32.895840	1.2±0.3	176±7	85	76.162483	32.754821	5.0±1.4	122±4
26	76.171562	32.843739	1.7±0.2	197±4	86	76.178909	32.777843	4.9 ± 1.0	126±11
27	76.182274	32.872364	3.6 ± 1.2	156±9	87	76.183281	32.788123	4.8±0.3	137±3
28	76.199074	32.869507	2.9 ± 0.6	181±6	88	76.194901	32.811313	4.3±0.7	141±7
29	75.954376	32.651176	0.6 ± 0.1	160±6	89	76.186783	32.746787	2.8±0.9	178±5
30	75.977623	32.659569	2.8±0.4	108±4	90	76.194557	32.762157	2.0 ± 0.9 2.1 ± 0.4	176±3 155±7
31	75.966957	32.614342	1.3 ± 0.3	141±5	91	76.207397	32.794330	1.7 ± 0.2	152±3
32	75.981514	32.604176	0.8 ± 0.2	178±6	92	76.199966	32.748481	4.6±0.5	91±3
33	75.989944	32.606697	1.7±0.3	148±6	93	76.221397	32.807666	3.6±0.4	204±2
34	75.999878	32.639458	2.0 ± 0.5	126±8	94	76.241035	32.813396	3.5 ± 0.7	73±11
35	76.022934	32.665119	0.9 ± 0.3	160±8			L1544		
36	76.023193	32.640354	1.4 ± 0.2	144±4			121344		
37	76.059883	32.638119	0.9 ± 0.2	145±6	1	76.057228	25.108257	1.2 ± 0.3	53±7
38	76.067558	32.642220	1.3 ± 0.2	169±3	2	76.089081	25.118418	2.1 ± 0.6	41±8
39	76.076180	32.606525	1.1 ± 0.3	189±7	3	76.127922	25.128275	1.9 ± 0.2	59±2
40	75.821548	32.718387	1.3 ± 0.1	138±1	4	76.125549	25.118435	1.8 ± 0.2	53±3
41	75.864555	32.755851	3.2 ± 0.2	142±2	5	76.113373	25.074015	1.0±0.3	42±8
42	75.880150	32.739234	1.7 ± 0.2	149±4	6	76.058960	25.038523	0.8 ± 0.2	88±5
43	75.874168	32.695308	1.0 ± 0.2	123±4	7	76.087753	25.030443	1.7±0.4	71±6
44	75.901093	32.746322	4.6±1.0	141±6	8	76.146156	25.052807	0.6 ± 0.2	63±8
45	75.886436	32.673606	1.8±0.4	123±7	9	76.145523	25.032807	1.8±0.5	47±8
46	75.915199	32.762527	1.4±0.1	153±2					
47	75.955101	32.713634	1.4±0.1 1.8±0.3	120±4	10	76.016464	25.107189	1.9±0.4	113±6
48	75.808868	32.820480	3.4 ± 0.5	169±4	11	76.057167	25.106194	1.8±0.4	90±6
					12	76.235374	25.302361	2.8±0.6	45±7
49	75.843201	32.868038	1.2 ± 0.2	156±4	13	76.251297	25.310106	2.3±0.4	49±5
50	75.838257	32.812008	2.2±0.3	169±4	14	76.260139	25.309694	2.8 ± 0.3	50±3
51	75.848991	32.847015	2.8±0.2	159±2	15	76.237396	25.291946	3.4 ± 0.1	57 ± 1
52	75.852913	32.813793	2.8±0.7	140±7	16	76.212265	25.276058	4.4 ± 1.4	48±9
53	75.861488	32.846989	6.4±1.6	160±7	17	76.275375	25.300722	2.6 ± 0.4	46±5
54	75.877274	32.864197	1.4±0.3	153±6	18	76.245178	25.283043	2.5 ± 0.5	47±5
55	75.869102	32.825848	2.9±0.3	158±3	19	76.281631	25.295921	2.6 ± 0.3	55±3
56	75.880882	32.863953	2.5 ± 0.5	159±6	20	76.193909	25.243095	5.6 ± 1.1	28 ± 5
57	75.890434	32.870522	6.3 ± 1.0	186±5	21	76.281998	25.287325	4.0 ± 1.1	74 ± 8
58	75.897346	32.882835	3.0 ± 0.7	144±6	22	76.234612	25.260841	3.1 ± 0.8	46±7
59	75.900948	32.874069	2.7 ± 0.1	151±1	23	76.290482	25.290985	2.2 ± 0.4	52±5
60	75.904366	32.846634	3.4 ± 0.3	160±3	24	76.237526	25.257521	2.8 ± 0.6	52±6
61	75.912674	32.835228	3.4 ± 0.2	154±1	25	76.245140	25.255503	3.3 ± 0.6	42±5
62	75.920509	32.860737	2.3 ± 0.6	131±7	26	76.308716	25.285637	2.3 ± 0.1	59±2
63	75.929703	32.813766	2.4 ± 0.8	148±9	27	76.296082	25.272753	4.1 ± 0.6	67±4
64	75.929123	32.806206	3.5 ± 0.7	188±6	28	76.304832	25.275841	3.3 ± 0.3	59±2
65	75.950523	32.854229	4.5 ± 0.3	164±2	29	76.256004	25.247278	3.4 ± 0.3	51±2
66	75.932022	32.878132	1.8 ± 0.1	155±2	30	76.315498	25.276484	2.1±0.5	65±6
67	75.943344	32.918541	2.2 ± 0.4	172±5	31	76.249496	25.238979	4.3 ± 0.2	57±1
68	75.933197	32.877018	1.9 ± 0.1	149±2	32	76.242897	25.227686	5.4 ± 0.6	48±3
69	75.959351	32.932571	1.5±0.4	160±7	33				
70	75.956909	32.909149	2.0 ± 0.3	172±5		76.254791	25.225065	2.5 ± 0.5	54±5
71	75.953285	32.889267	1.6±0.3	165±4	34	76.261375	25.228199	2.5±0.6	55±7
72	75.933283	32.904507	1.0±0.3 1.8±0.1	149±1	35	76.273216	25.229153	1.8±0.6	77±9
73	75.992607				36	76.242256	25.207714	3.5 ± 0.1	51±1
		32.935608	3.0 ± 0.9	115±8	37	76.279312	25.219023	3.2±0.2	59±2
74	75.998016	32.899822	2.3 ± 0.6	162±7	38	76.256058	25.197462	2.3±0.6	60±7
75	76.021591	32.930729	2.4 ± 0.7	169±8	39	76.062073	25.373821	1.4 ± 0.4	91±8
76	76.034760	32.928242	1.5±0.5	145±9	40	76.071907	25.377256	2.4 ± 0.6	52±7
77	76.056839	32.925343	1.0±0.3	160±7	41	76.076889	25.369682	2.1 ± 0.3	51±3
78	76.124908	32.772536	1.3±0.3	135±15	42	76.067070	25.357315	4.7 ± 0.8	44±5
79	76.142113	32.788318	4.1±1.1	207±9	43	76.087212	25.360737	1.5 ± 0.3	46±6
					44	76.035110	25.325567	4.5 ± 1.0	43±6

45	76.072121	25.336781	2.7±0.5	57±5		105	75.814072	25.285645	3.3±0.2	75±2
46	76.068024	25.315220	4.0 ± 0.8	78±6		106	75.822998	25.290022	3.4 ± 0.2	75±2
47	76.117973	25.328358	3.6 ± 0.5	48±4		107	75.758423	25.252281	3.5±0.5	89±4
48	76.065918	25.289679	4.9±1.2	33±7		108	75.831055	25.274052	3.1 ± 1.0	92±9
49	76.030487	25.368849	6.0±0.9	58±4		109	75.847015	25.280731	3.2±0.6	73±6
50	76.078751	25.393486	1.4±0.4	48±7		110	75.813591	25.258505	1.7±0.5	59±9
51	76.062080	25.373770	1.7±0.7	41±3		111	75.782776	25.233969	4.3±0.8	56±5
52	76.071846	25.377312	2.2±0.2	45±3		112	75.791924	25.236813	2.8±0.3	86±3
53	76.076851	25.369694	2.2±0.2 2.2±0.1	51±1		113	75.816910	25.248405	0.6 ± 0.2	74±7
54	76.067055	25.357246	2.3 ± 0.3	51±1 51±4		114	75.787399	25.231300	2.3±0.4	83±5
55	76.097504	25.371729	2.9 ± 0.3 2.9 ± 0.4	46±4		115	75.804199	25.237904	2.7±0.3	72±3
56	76.030022	25.333433	3.0 ± 0.9	60±8		116	75.856033	25.265120	3.8 ± 0.7	67±6
57	76.030022	25.360748	2.5±0.9	47±1		117	75.831566	25.265120	3.8±0.7 2.4±0.4	72±4
58										
59	76.035072	25.325525	3.6 ± 0.4	52±3		118	75.815590	25.235275	1.9 ± 0.2	74±2
	76.126968	25.374454	4.4 ± 0.7	31±5		119	75.791939	25.221834	2.9 ± 0.2	70±2
60	76.095612	25.354708	2.8±0.6	67±6		120	75.806465	25.226585	4.1 ± 0.9	69±6
61	76.127930	25.370354	2.3±0.6	48±8		121	75.843140	25.240055	3.1 ± 0.2	71±2
62	76.118904	25.365253	3.7±0.8	9±6		122	75.854790	25.239071	2.6±0.3	79±4
63	76.072105	25.336784	2.9±0.2	60±2		123	75.859070	25.240129	3.2±0.8	95±7
64	76.025940	25.311419	5.3±1.3	88±7		124	75.848190	25.234303	3.3±0.1	72±1
65	76.071793	25.327324	3.3 ± 0.9	47±8		125	75.982834	25.473400	3.4 ± 0.8	86±5
66	76.068031	25.315233	2.6 ± 0.3	58±4		126	76.000893	25.480186	2.6 ± 0.4	68±3
67	76.117889	25.328384	3.4 ± 0.2	45 ± 2		127	76.024300	25.492476	7.4 ± 0.9	94 ± 3
68	76.087990	25.312168	2.9 ± 0.6	49±6		128	75.947830	25.432013	1.1 ± 0.2	69±4
69	76.097466	25.315281	2.4 ± 0.5	54±6		129	76.021156	25.466976	2.5 ± 0.4	66±4
70	76.091049	25.306902	2.9 ± 0.5	46±4		130	76.031769	25.471401	2.0 ± 0.4	58±6
71	76.137878	25.331186	3.7 ± 0.2	46 ± 1		131	75.967308	25.429609	1.0 ± 0.3	66±7
72	76.085701	25.302130	3.2 ± 0.9	53±8		132	75.978424	25.424036	2.2 ± 0.7	71±7
73	76.065910	25.289625	2.4 ± 0.6	35 ± 7		133	76.050774	25.444368	2.7 ± 0.5	79 ± 4
74	76.138542	25.324404	3.1 ± 0.5	42 ± 5		134	76.010574	25.416071	1.3 ± 0.3	59±6
75	76.126183	25.313448	3.5 ± 0.7	48±5		135	76.032639	25.419542	1.3 ± 0.3	57±6
75 76	76.126183 76.134743	25.313448 25.309156	3.5±0.7 4.4±1.2	48±5 74±8		135 136	76.032639 75.998466	25.419542 25.400034	1.3±0.3 1.5±0.4	
					,			25.400034		57±6
76	76.134743	25.309156	4.4 ± 1.2	74±8						57±6
76 77	76.134743 75.914574	25.309156 25.233492	4.4±1.2 9.4±1.0	74±8 61±3		136	75.998466	25.400034 L1523	1.5±0.4	57±6 55±8
76 77 78	76.134743 75.914574 75.875015	25.309156 25.233492 25.201035	4.4±1.2 9.4±1.0 6.2±1.2	74±8 61±3 80±5		136	75.998466 76.510254	25.400034 L1523 31.877089	1.5±0.4 2.1±0.2	57±6 55±8 117±2
76 77 78 79	76.134743 75.914574 75.875015 75.943802	25.309156 25.233492 25.201035 25.230867	4.4±1.2 9.4±1.0 6.2±1.2 6.1±0.8	74±8 61±3 80±5 67±3		136 1 2	75.998466 76.510254 76.527199	25.400034 L1523 31.877089 31.875944	1.5±0.4 2.1±0.2 2.2±0.1	57±6 55±8 117±2 147±1
76 77 78 79 80	76.134743 75.914574 75.875015 75.943802 75.876350	25.309156 25.233492 25.201035 25.230867 25.193361	4.4±1.2 9.4±1.0 6.2±1.2 6.1±0.8 3.7±1.0	74±8 61±3 80±5 67±3 61±8		136 1 2 3	75.998466 76.510254 76.527199 76.524780	25.400034 L1523 31.877089 31.875944 31.849361	1.5±0.4 2.1±0.2 2.2±0.1 7.8±2.0	57±6 55±8 117±2 147±1 116±8
76 77 78 79 80 81	76.134743 75.914574 75.875015 75.943802 75.876350 75.877235	25.309156 25.233492 25.201035 25.230867 25.193361 25.189051	4.4±1.2 9.4±1.0 6.2±1.2 6.1±0.8 3.7±1.0 3.1±0.5	74±8 61±3 80±5 67±3 61±8 67±5		136 1 2 3 4	75.998466 76.510254 76.527199 76.524780 76.530388	25.400034 L1523 31.877089 31.875944 31.849361 31.869553	1.5±0.4 2.1±0.2 2.2±0.1 7.8±2.0 2.2±0.4	57±6 55±8 117±2 147±1 116±8 139±5
76 77 78 79 80 81 82	76.134743 75.914574 75.875015 75.943802 75.876350 75.877235 75.949387	25.309156 25.233492 25.201035 25.230867 25.193361 25.189051 25.220924	4.4±1.2 9.4±1.0 6.2±1.2 6.1±0.8 3.7±1.0 3.1±0.5 5.4±0.4	74±8 61±3 80±5 67±3 61±8 67±5 63±2		136 1 2 3 4 5	75.998466 76.510254 76.527199 76.524780 76.530388 76.554489	25.400034 L1523 31.877089 31.875944 31.849361 31.869553 31.951887	2.1±0.2 2.2±0.1 7.8±2.0 2.2±0.4 5.7±1.6	57±6 55±8 117±2 147±1 116±8 139±5 122±9
76 77 78 79 80 81 82 83	76.134743 75.914574 75.875015 75.943802 75.876350 75.877235 75.949387 75.891914 75.943237	25.309156 25.233492 25.201035 25.230867 25.193361 25.189051 25.220924 25.187262	4.4±1.2 9.4±1.0 6.2±1.2 6.1±0.8 3.7±1.0 3.1±0.5 5.4±0.4 2.8±0.5	74±8 61±3 80±5 67±3 61±8 67±5 63±2 66±5		136 1 2 3 4 5 6	75.998466 76.510254 76.527199 76.524780 76.530388 76.554489 76.537842	25.400034 L1523 31.877089 31.875944 31.849361 31.869553 31.951887 31.850721	1.5±0.4 2.1±0.2 2.2±0.1 7.8±2.0 2.2±0.4 5.7±1.6 2.5±0.3	57±6 55±8 117±2 147±1 116±8 139±5 122±9 153±3
76 77 78 79 80 81 82 83 84 85	76.134743 75.914574 75.875015 75.943802 75.876350 75.877235 75.949387 75.891914 75.943237 75.877106	25.309156 25.233492 25.201035 25.230867 25.193361 25.189051 25.220924 25.187262 25.202789 25.151016	4.4±1.2 9.4±1.0 6.2±1.2 6.1±0.8 3.7±1.0 3.1±0.5 5.4±0.4 2.8±0.5 5.4±0.5 2.8±0.4	74±8 61±3 80±5 67±3 61±8 67±5 63±2 66±5 61±3 64±3		136 1 2 3 4 5 6 7	75.998466 76.510254 76.527199 76.524780 76.530388 76.554489 76.537842 76.568336	25.400034 L1523 31.877089 31.875944 31.849361 31.869553 31.951887 31.850721 31.914982	2.1±0.2 2.2±0.1 7.8±2.0 2.2±0.4 5.7±1.6 2.5±0.3 2.7±0.5	57±6 55±8 117±2 147±1 116±8 139±5 122±9 153±3 157±5
76 77 78 79 80 81 82 83 84	76.134743 75.914574 75.875015 75.943802 75.876350 75.877235 75.949387 75.891914 75.943237	25.309156 25.233492 25.201035 25.230867 25.193361 25.189051 25.220924 25.187262 25.202789	4.4±1.2 9.4±1.0 6.2±1.2 6.1±0.8 3.7±1.0 3.1±0.5 5.4±0.4 2.8±0.5 5.4±0.5	74±8 61±3 80±5 67±3 61±8 67±5 63±2 66±5 61±3 64±3		136 1 2 3 4 5 6 7 8	75.998466 76.510254 76.527199 76.524780 76.530388 76.554489 76.537842 76.568336 76.569550	25.400034 L1523 31.877089 31.875944 31.849361 31.869553 31.951887 31.850721 31.914982 31.917919	2.1±0.2 2.2±0.1 7.8±2.0 2.2±0.4 5.7±1.6 2.5±0.3 2.7±0.5 2.3±0.2	57±6 55±8 117±2 147±1 116±8 139±5 122±9 153±3 157±5 136±2
76 77 78 79 80 81 82 83 84 85 86 87	76.134743 75.914574 75.875015 75.943802 75.876350 75.877235 75.949387 75.891914 75.943237 75.877106 75.942673	25.309156 25.233492 25.201035 25.230867 25.193361 25.189051 25.220924 25.187262 25.202789 25.151016 25.182020	4.4±1.2 9.4±1.0 6.2±1.2 6.1±0.8 3.7±1.0 3.1±0.5 5.4±0.4 2.8±0.5 5.4±0.5 2.8±0.4 4.3±0.6 3.7±0.4	74±8 61±3 80±5 67±3 61±8 67±5 63±2 66±5 61±3 64±3 68±4 62±3		136 1 2 3 4 5 6 7 8 9	75.998466 76.510254 76.527199 76.524780 76.530388 76.554489 76.537842 76.568336 76.569550 76.595695	25.400034 L1523 31.877089 31.875944 31.849361 31.869553 31.951887 31.850721 31.914982 31.917919 31.941668	2.1±0.2 2.2±0.1 7.8±2.0 2.2±0.4 5.7±1.6 2.5±0.3 2.7±0.5 2.3±0.2 2.4±0.4	57±6 55±8 117±2 147±1 116±8 139±5 122±9 153±3 157±5 136±2 125±6
76 77 78 79 80 81 82 83 84 85 86 87 88	76.134743 75.914574 75.875015 75.943802 75.876350 75.877235 75.949387 75.891914 75.943237 75.877106 75.942673 75.980614 75.935455	25.309156 25.233492 25.201035 25.230867 25.193361 25.189051 25.220924 25.187262 25.202789 25.151016 25.182020 25.184624 25.154423	4.4±1.2 9.4±1.0 6.2±1.2 6.1±0.8 3.7±1.0 3.1±0.5 5.4±0.4 2.8±0.5 5.4±0.5 2.8±0.4 4.3±0.6 3.7±0.4 3.7±0.7	74±8 61±3 80±5 67±3 61±8 67±5 63±2 66±5 61±3 64±3 68±4 62±3 67±5		136 1 2 3 4 5 6 7 8 9 10	75.998466 76.510254 76.527199 76.524780 76.530388 76.554489 76.537842 76.568336 76.569550 76.595695 76.616318	25.400034 L1523 31.877089 31.875944 31.849361 31.869553 31.951887 31.850721 31.914982 31.917919 31.941668 31.913567	2.1±0.2 2.2±0.1 7.8±2.0 2.2±0.4 5.7±1.6 2.5±0.3 2.7±0.5 2.3±0.2 2.4±0.4 2.3±0.7	57±6 55±8 117±2 147±1 116±8 139±5 122±9 153±3 157±5 136±2 125±6 149±9
76 77 78 79 80 81 82 83 84 85 86 87 88	76.134743 75.914574 75.875015 75.943802 75.876350 75.877235 75.949387 75.891914 75.943237 75.877106 75.942673 75.980614 75.935455 75.891846	25.309156 25.233492 25.201035 25.230867 25.193361 25.189051 25.220924 25.187262 25.202789 25.151016 25.182020 25.184624 25.154423 25.129160	4.4±1.2 9.4±1.0 6.2±1.2 6.1±0.8 3.7±1.0 3.1±0.5 5.4±0.4 2.8±0.5 5.4±0.5 2.8±0.4 4.3±0.6 3.7±0.4 3.7±0.7 3.6±0.8	74±8 61±3 80±5 67±3 61±8 67±5 63±2 66±5 61±3 64±3 68±4 62±3 67±5 73±6		136 1 2 3 4 5 6 7 8 9 10 11	75.998466 76.510254 76.527199 76.524780 76.530388 76.554489 76.537842 76.568336 76.569550 76.595695 76.616318 76.611382	25.400034 L1523 31.877089 31.875944 31.849361 31.869553 31.951887 31.850721 31.914982 31.917919 31.941668 31.913567 31.873421	2.1±0.2 2.2±0.1 7.8±2.0 2.2±0.4 5.7±1.6 2.5±0.3 2.7±0.5 2.3±0.2 2.4±0.4 2.3±0.7 3.3±0.4	57±6 55±8 117±2 147±1 116±8 139±5 122±9 153±3 157±5 136±2 125±6 149±9 154±3
76 77 78 79 80 81 82 83 84 85 86 87 88 89	76.134743 75.914574 75.875015 75.943802 75.876350 75.877235 75.949387 75.891914 75.943237 75.877106 75.942673 75.980614 75.935455 75.891846 75.961937	25.309156 25.233492 25.201035 25.230867 25.193361 25.189051 25.220924 25.187262 25.202789 25.151016 25.182020 25.184624 25.154423 25.129160 25.160721	4.4±1.2 9.4±1.0 6.2±1.2 6.1±0.8 3.7±1.0 3.1±0.5 5.4±0.4 2.8±0.5 5.4±0.5 2.8±0.4 4.3±0.6 3.7±0.4 3.7±0.7 3.6±0.8 3.5±1.0	74±8 61±3 80±5 67±3 61±8 67±5 63±2 66±5 61±3 64±3 68±4 62±3 67±5 73±6 60±8		136 1 2 3 4 5 6 7 8 9 10 11 12	75.998466 76.510254 76.527199 76.524780 76.530388 76.554489 76.568336 76.569550 76.595695 76.616318 76.611382 76.362289	25.400034 L1523 31.877089 31.875944 31.849361 31.869553 31.951887 31.850721 31.914982 31.917919 31.941668 31.913567 31.873421 31.808458	2.1±0.2 2.2±0.1 7.8±2.0 2.2±0.4 5.7±1.6 2.5±0.3 2.7±0.5 2.3±0.2 2.4±0.4 2.3±0.7 3.3±0.4 1.5±0.4	57±6 55±8 117±2 147±1 116±8 139±5 122±9 153±3 157±5 136±2 125±6 149±9 154±3 139±8
76 77 78 79 80 81 82 83 84 85 86 87 88 89 90	76.134743 75.914574 75.875015 75.943802 75.876350 75.877235 75.949387 75.891914 75.943237 75.877106 75.942673 75.980614 75.935455 75.891846 75.961937 75.912445	25.309156 25.233492 25.201035 25.230867 25.193361 25.189051 25.220924 25.187262 25.202789 25.151016 25.182020 25.184624 25.154423 25.129160 25.160721 25.127752	4.4±1.2 9.4±1.0 6.2±1.2 6.1±0.8 3.7±1.0 3.1±0.5 5.4±0.4 2.8±0.5 5.4±0.5 2.8±0.4 4.3±0.6 3.7±0.4 3.7±0.7 3.6±0.8 3.5±1.0 3.0±0.8	74±8 61±3 80±5 67±3 61±8 67±5 63±2 66±5 61±3 64±3 67±5 73±6 60±8 61±8		136 1 2 3 4 5 6 7 8 9 10 11 12 13	75.998466 76.510254 76.527199 76.524780 76.530388 76.554489 76.568336 76.569550 76.595695 76.616318 76.611382 76.362289 76.369514	25.400034 L1523 31.877089 31.875944 31.849361 31.869553 31.951887 31.850721 31.914982 31.917919 31.941668 31.913567 31.873421 31.808458 31.820160	2.1±0.2 2.2±0.1 7.8±2.0 2.2±0.4 5.7±1.6 2.5±0.3 2.7±0.5 2.3±0.2 2.4±0.4 2.3±0.7 3.3±0.4 1.5±0.4 2.3±0.6	57±6 55±8 117±2 147±1 116±8 139±5 122±9 153±3 157±5 136±2 125±6 149±9 154±3 139±8 133±7
76 77 78 79 80 81 82 83 84 85 86 87 88 89 90 91	76.134743 75.914574 75.875015 75.943802 75.876350 75.877235 75.949387 75.891914 75.943237 75.877106 75.942673 75.980614 75.935455 75.891846 75.961937 75.912445 75.940964	25.309156 25.233492 25.201035 25.230867 25.193361 25.189051 25.220924 25.187262 25.202789 25.151016 25.182020 25.184624 25.154423 25.129160 25.160721 25.127752 25.139061	4.4±1.2 9.4±1.0 6.2±1.2 6.1±0.8 3.7±1.0 3.1±0.5 5.4±0.4 2.8±0.5 5.4±0.5 2.8±0.4 4.3±0.6 3.7±0.4 3.7±0.7 3.6±0.8 3.5±1.0 3.0±0.8 2.9±0.3	74±8 61±3 80±5 67±3 61±8 67±5 63±2 66±5 61±3 64±3 68±4 62±3 67±5 73±6 60±8 61±8 61±3		136 1 2 3 4 5 6 7 8 9 10 11 12 13 14	75.998466 76.510254 76.527199 76.524780 76.530388 76.554489 76.537842 76.568336 76.569550 76.595695 76.616318 76.611382 76.362289 76.369514 76.380829	25.400034 L1523 31.877089 31.875944 31.849361 31.869553 31.951887 31.850721 31.914982 31.917919 31.941668 31.913567 31.873421 31.808458 31.820160 31.780537	2.1±0.2 2.2±0.1 7.8±2.0 2.2±0.4 5.7±1.6 2.5±0.3 2.7±0.5 2.3±0.2 2.4±0.4 2.3±0.7 3.3±0.4 1.5±0.4 2.3±0.6 1.7±0.1	57±6 55±8 117±2 147±1 116±8 139±5 122±9 153±3 157±5 136±2 125±6 149±9 154±3 139±8 133±7 127±2
76 77 78 79 80 81 82 83 84 85 86 87 88 89 90 91 92 93	76.134743 75.914574 75.875015 75.943802 75.876350 75.877235 75.949387 75.891914 75.943237 75.877106 75.942673 75.980614 75.935455 75.891846 75.961937 75.912445 75.940964 75.774246	25.309156 25.233492 25.201035 25.230867 25.193361 25.189051 25.220924 25.187262 25.202789 25.151016 25.182020 25.184624 25.154423 25.129160 25.160721 25.127752 25.139061 25.314596	4.4±1.2 9.4±1.0 6.2±1.2 6.1±0.8 3.7±1.0 3.1±0.5 5.4±0.4 2.8±0.5 5.4±0.5 2.8±0.4 4.3±0.6 3.7±0.4 3.7±0.7 3.6±0.8 3.5±1.0 3.0±0.8 2.9±0.3 2.8±0.6	74±8 61±3 80±5 67±3 61±8 67±5 63±2 66±5 61±3 64±3 67±5 73±6 60±8 61±8 61±3 66±6		136 1 2 3 4 5 6 7 8 9 10 11 12 13 14 15	75.998466 76.510254 76.527199 76.524780 76.530388 76.554489 76.537842 76.568336 76.569550 76.616318 76.611382 76.362289 76.369514 76.380829 76.390350	25.400034 L1523 31.877089 31.875944 31.849361 31.869553 31.951887 31.850721 31.914982 31.917919 31.941668 31.913567 31.873421 31.808458 31.820160 31.780537 31.807999	2.1±0.2 2.2±0.1 7.8±2.0 2.2±0.4 5.7±1.6 2.5±0.3 2.7±0.5 2.3±0.2 2.4±0.4 2.3±0.7 3.3±0.4 1.5±0.4 2.3±0.6 1.7±0.1 2.1±0.5	57±6 55±8 117±2 147±1 116±8 139±5 122±9 153±3 157±5 136±2 125±6 149±9 154±3 139±8 133±7 127±2 132±7
76 77 78 79 80 81 82 83 84 85 86 87 88 89 90 91 92 93 94	76.134743 75.914574 75.875015 75.943802 75.876350 75.877235 75.949387 75.891914 75.943237 75.877106 75.942673 75.980614 75.935455 75.891846 75.961937 75.912445 75.940964 75.774246 75.779404	25.309156 25.233492 25.201035 25.230867 25.193361 25.189051 25.220924 25.187262 25.202789 25.151016 25.182020 25.184624 25.154423 25.129160 25.160721 25.127752 25.139061 25.314596 25.304075	4.4±1.2 9.4±1.0 6.2±1.2 6.1±0.8 3.7±1.0 3.1±0.5 5.4±0.4 2.8±0.5 5.4±0.5 2.8±0.4 4.3±0.6 3.7±0.7 3.6±0.8 3.5±1.0 3.0±0.8 2.9±0.3 2.8±0.6 2.8±0.3	74±8 61±3 80±5 67±3 61±8 67±5 63±2 66±5 61±3 64±3 67±5 73±6 60±8 61±8 61±3 66±6 78±3		136 1 2 3 4 5 6 7 8 9 10 11 12 13 14 15 16	75.998466 76.510254 76.527199 76.524780 76.530388 76.554489 76.537842 76.568336 76.569550 76.616318 76.611382 76.362289 76.369514 76.380829 76.390350 76.405693	25.400034 L1523 31.877089 31.875944 31.849361 31.869553 31.951887 31.850721 31.914982 31.917919 31.941668 31.913567 31.873421 31.808458 31.820160 31.780537 31.807999 31.815182	2.1±0.2 2.2±0.1 7.8±2.0 2.2±0.4 5.7±1.6 2.5±0.3 2.7±0.5 2.3±0.2 2.4±0.4 2.3±0.7 3.3±0.4 1.5±0.4 2.3±0.6 1.7±0.1 2.1±0.5 3.0±0.5	117±2 147±1 116±8 139±5 122±9 153±3 157±5 136±2 125±6 149±9 154±3 139±8 133±7 127±2 132±7 140±4
76 77 78 79 80 81 82 83 84 85 86 87 88 89 90 91 92 93 94 95	76.134743 75.914574 75.875015 75.943802 75.876350 75.877235 75.949387 75.943237 75.877106 75.942673 75.980614 75.935455 75.912445 75.912445 75.940964 75.774246 75.779404 75.7737396	25.309156 25.233492 25.201035 25.230867 25.193361 25.189051 25.220924 25.187262 25.202789 25.151016 25.182020 25.184624 25.154423 25.129160 25.160721 25.127752 25.139061 25.314596 25.304075 25.280252	4.4±1.2 9.4±1.0 6.2±1.2 6.1±0.8 3.7±1.0 3.1±0.5 5.4±0.4 2.8±0.5 5.4±0.5 2.8±0.4 4.3±0.6 3.7±0.4 3.7±0.7 3.6±0.8 3.5±1.0 3.0±0.8 2.9±0.3 2.8±0.6 2.8±0.3 2.1±0.4	74±8 61±3 80±5 67±3 61±8 67±5 63±2 66±5 61±3 64±3 67±5 73±6 60±8 61±8 61±3 66±6 78±3 78±6		136 1 2 3 4 5 6 7 8 9 10 11 12 13 14 15 16 17	75.998466 76.510254 76.527199 76.524780 76.530388 76.554489 76.537842 76.568336 76.569550 76.595695 76.616318 76.611382 76.362289 76.369514 76.380829 76.390350 76.405693 76.405693 76.430855	25.400034 L1523 31.877089 31.875944 31.849361 31.869553 31.951887 31.850721 31.914982 31.917919 31.941668 31.913567 31.873421 31.808458 31.820160 31.780537 31.807999 31.815182 31.839384	2.1±0.2 2.2±0.1 7.8±2.0 2.2±0.4 5.7±1.6 2.5±0.3 2.7±0.5 2.3±0.2 2.4±0.4 2.3±0.7 3.3±0.4 1.5±0.4 2.3±0.5 3.0±0.5 3.0±0.5 3.8±0.9	57±6 55±8 117±2 147±1 116±8 139±5 122±9 153±3 157±5 136±2 125±6 149±9 154±3 139±8 133±7 127±2 132±7 140±4 133±6
76 77 78 79 80 81 82 83 84 85 86 87 88 89 90 91 92 93 94 95 96	76.134743 75.914574 75.875015 75.943802 75.876350 75.877235 75.949387 75.943237 75.877106 75.942673 75.980614 75.935455 75.912445 75.912445 75.940964 75.774246 75.779404 75.737396 75.768265	25.309156 25.233492 25.201035 25.230867 25.193361 25.189051 25.220924 25.187262 25.202789 25.151016 25.182020 25.184624 25.154423 25.129160 25.160721 25.127752 25.139061 25.314596 25.304075 25.280252 25.294556	4.4±1.2 9.4±1.0 6.2±1.2 6.1±0.8 3.7±1.0 3.1±0.5 5.4±0.4 2.8±0.5 5.4±0.5 2.8±0.4 4.3±0.6 3.7±0.4 3.7±0.7 3.6±0.8 3.5±1.0 3.0±0.8 2.9±0.3 2.8±0.6 2.8±0.4 4.3±0.6 4.3	74±8 61±3 80±5 67±3 61±8 67±5 63±2 66±5 61±3 64±3 67±5 73±6 60±8 61±8 61±3 66±6 78±3 78±6 86±7		136 1 2 3 4 5 6 7 8 9 10 11 12 13 14 15 16 17 18	75.998466 76.510254 76.527199 76.524780 76.530388 76.554489 76.537842 76.568336 76.569550 76.595695 76.616318 76.611382 76.362289 76.369514 76.380829 76.390350 76.405693 76.405693 76.430855 76.418915	25.400034 L1523 31.877089 31.875944 31.849361 31.869553 31.951887 31.850721 31.914982 31.917919 31.941668 31.913567 31.873421 31.808458 31.820160 31.780537 31.807999 31.815182 31.839384 31.760109	2.1±0.2 2.2±0.1 7.8±2.0 2.2±0.4 5.7±1.6 2.5±0.3 2.7±0.5 2.3±0.2 2.4±0.4 2.3±0.7 3.3±0.4 1.5±0.4 2.1±0.5 3.0±0.5 3.8±0.9 1.3±0.2	57±6 55±8 117±2 147±1 116±8 139±5 122±9 153±3 157±5 136±2 125±6 149±9 154±3 139±8 133±7 127±2 132±7 140±4 133±6 147±4
76 77 78 79 80 81 82 83 84 85 86 87 88 89 90 91 92 93 94 95 96 97	76.134743 75.914574 75.875015 75.943802 75.876350 75.877235 75.949387 75.943237 75.877106 75.942673 75.980614 75.935455 75.891846 75.961937 75.912445 75.940964 75.774246 75.779404 75.737396 75.768265 75.810715	25.309156 25.233492 25.201035 25.230867 25.193361 25.189051 25.220924 25.187262 25.202789 25.151016 25.182020 25.184624 25.154423 25.129160 25.160721 25.127752 25.139061 25.314596 25.304075 25.280252 25.294556 25.317068	4.4±1.2 9.4±1.0 6.2±1.2 6.1±0.8 3.7±1.0 3.1±0.5 5.4±0.4 2.8±0.5 5.4±0.5 2.8±0.4 4.3±0.6 3.7±0.4 3.7±0.7 3.6±0.8 2.9±0.3 2.8±0.6 2.8±0.3 2.1±0.4 2.4±0.6 3.1±0.6	74±8 61±3 80±5 67±3 61±8 67±5 63±2 66±5 61±3 64±3 67±5 73±6 60±8 61±3 66±6 78±3 78±6 86±7 72±5		136 1 2 3 4 5 6 7 8 9 10 11 12 13 14 15 16 17 18 19	75.998466 76.510254 76.527199 76.524780 76.530388 76.554489 76.568336 76.569550 76.595695 76.616318 76.611382 76.362289 76.369514 76.380829 76.390350 76.405693 76.405693 76.430855 76.418915 76.455315	25.400034 L1523 31.877089 31.875944 31.849361 31.869553 31.951887 31.850721 31.914982 31.917919 31.941668 31.913567 31.873421 31.808458 31.820160 31.780537 31.807999 31.815182 31.839384 31.760109 31.829580	2.1±0.2 2.2±0.1 7.8±2.0 2.2±0.4 5.7±1.6 2.5±0.3 2.7±0.5 2.3±0.2 2.4±0.4 2.3±0.7 3.3±0.4 1.5±0.4 2.3±0.5 3.0±0.5 3.8±0.9 1.3±0.2 2.5±0.3	57±6 55±8 117±2 147±1 116±8 139±5 122±9 153±3 157±5 136±2 125±6 149±9 154±3 139±8 133±7 127±2 132±7 140±4 133±6 147±4 136±3
76 77 78 79 80 81 82 83 84 85 86 87 88 89 90 91 92 93 94 95 96 97 98	76.134743 75.914574 75.875015 75.943802 75.876350 75.877235 75.949387 75.943237 75.877106 75.942673 75.980614 75.935455 75.891846 75.961937 75.912445 75.74246 75.774246 75.779404 75.77396 75.768265 75.810715 75.808716	25.309156 25.233492 25.201035 25.230867 25.193361 25.189051 25.220924 25.187262 25.202789 25.151016 25.182020 25.184624 25.154423 25.129160 25.160721 25.127752 25.139061 25.314596 25.304075 25.280252 25.294556 25.317068 25.302570	4.4±1.2 9.4±1.0 6.2±1.2 6.1±0.8 3.7±1.0 3.1±0.5 5.4±0.4 2.8±0.5 5.4±0.5 2.8±0.4 4.3±0.6 3.7±0.4 3.7±0.7 3.6±0.8 2.9±0.3 2.8±0.6 2.8±0.3 2.1±0.4 2.4±0.6 3.1±0.6 3.3±0.2	74±8 61±3 80±5 67±3 61±8 67±5 63±2 66±5 61±3 64±3 67±5 73±6 60±8 61±8 61±3 66±6 78±3 78±6 86±7 72±5 66±2		136 1 2 3 4 5 6 7 8 9 10 11 12 13 14 15 16 17 18 19 20	75.998466 76.510254 76.527199 76.524780 76.530388 76.554489 76.537842 76.568336 76.569550 76.595695 76.616318 76.362289 76.369514 76.380829 76.390350 76.405693 76.405693 76.430855 76.418915 76.455315 76.447815	25.400034 L1523 31.877089 31.875944 31.849361 31.869553 31.951887 31.850721 31.914982 31.917919 31.941668 31.913567 31.873421 31.808458 31.820160 31.780537 31.807999 31.815182 31.839384 31.760109 31.829580 31.797075	2.1±0.2 2.2±0.1 7.8±2.0 2.2±0.4 5.7±1.6 2.5±0.3 2.7±0.5 2.3±0.2 2.4±0.4 2.3±0.7 3.3±0.4 1.5±0.4 2.3±0.5 3.0±0.5 3.8±0.9 1.3±0.2 2.5±0.3 2.1±0.6	57±6 55±8 117±2 147±1 116±8 139±5 122±9 153±3 157±5 136±2 125±6 149±9 154±3 139±8 133±7 127±2 132±7 140±4 133±6 147±4 136±3 142±7
76 77 78 79 80 81 82 83 84 85 86 87 88 89 90 91 92 93 94 95 96 97 98	76.134743 75.914574 75.875015 75.943802 75.876350 75.877235 75.949387 75.943237 75.877106 75.942673 75.980614 75.935455 75.891846 75.961937 75.912445 75.774246 75.774246 75.774246 75.7737396 75.768265 75.810715 75.808716 75.734344	25.309156 25.233492 25.201035 25.230867 25.193361 25.189051 25.220924 25.187262 25.202789 25.151016 25.182020 25.184624 25.154423 25.129160 25.160721 25.127752 25.139061 25.304075 25.280252 25.294556 25.317068 25.302570 25.261499	4.4±1.2 9.4±1.0 6.2±1.2 6.1±0.8 3.7±1.0 3.1±0.5 5.4±0.4 2.8±0.5 5.4±0.5 2.8±0.4 4.3±0.6 3.7±0.4 3.7±0.7 3.6±0.8 2.9±0.3 2.8±0.6 2.8±0.3 2.1±0.4 2.4±0.6 3.1±0.6 3.1±0.6 3.1±0.4 2.4±0.6 3.1±0.8	74±8 61±3 80±5 67±3 61±8 67±5 63±2 66±5 61±3 64±3 67±5 73±6 60±8 61±8 61±3 66±6 78±3 78±6 86±7 72±5 66±2 74±3		136 1 2 3 4 5 6 7 8 9 10 11 12 13 14 15 16 17 18 19 20 21	75.998466 76.510254 76.527199 76.524780 76.530388 76.554489 76.568336 76.569550 76.595695 76.616318 76.369289 76.369514 76.380829 76.390350 76.405693 76.405693 76.430855 76.418915 76.447815 76.447815 76.451042	25.400034 L1523 31.877089 31.875944 31.849361 31.869553 31.951887 31.850721 31.914982 31.917919 31.941668 31.913567 31.873421 31.808458 31.820160 31.780537 31.807999 31.815182 31.839384 31.760109 31.829580 31.797075 31.766788	2.1±0.2 2.2±0.1 7.8±2.0 2.2±0.4 5.7±1.6 2.5±0.3 2.7±0.5 2.3±0.2 2.4±0.4 2.3±0.7 3.3±0.4 1.5±0.4 2.3±0.5 3.0±0.5 3.8±0.9 1.3±0.2 2.5±0.3 2.1±0.6 2.1±0.5	57±6 55±8 117±2 147±1 116±8 139±5 122±9 153±3 157±5 136±2 125±6 149±9 154±3 139±8 133±7 127±2 132±7 140±4 133±6 147±4 136±3 142±7 129±7
76 77 78 79 80 81 82 83 84 85 86 87 88 89 90 91 92 93 94 95 96 97 98 99 100	76.134743 75.914574 75.875015 75.943802 75.876350 75.877235 75.949387 75.891914 75.943237 75.877106 75.942673 75.980614 75.935455 75.891846 75.961937 75.912445 75.774246 75.774246 75.774246 75.775940964 75.775940964 75.775940964 75.7759404 75.77594 75.77594 75.77594 75.77594 75.77594 75.77594 75.	25.309156 25.233492 25.201035 25.230867 25.193361 25.189051 25.220924 25.187262 25.202789 25.151016 25.182020 25.184624 25.154423 25.129160 25.160721 25.127752 25.314596 25.304075 25.280252 25.294556 25.317068 25.302570 25.261499 25.287922	4.4±1.2 9.4±1.0 6.2±1.2 6.1±0.8 3.7±1.0 3.1±0.5 5.4±0.4 2.8±0.5 5.4±0.5 2.8±0.4 4.3±0.6 3.7±0.4 3.7±0.7 3.6±0.8 2.9±0.3 2.8±0.6 2.8±0.3 2.1±0.4 2.4±0.6 3.1±0.6 3.3±0.2 1.8±0.2 2.1±0.5	74±8 61±3 80±5 67±3 61±8 67±5 63±2 66±5 61±3 64±3 67±5 73±6 60±8 61±8 61±3 66±6 78±3 78±6 86±7 72±5 66±2 74±3 73±7		136 1 2 3 4 5 6 7 8 9 10 11 12 13 14 15 16 17 18 19 20 21 22	75.998466 76.510254 76.527199 76.524780 76.530388 76.554489 76.568336 76.569550 76.595695 76.616318 76.369289 76.369514 76.380829 76.390350 76.405693 76.405693 76.455315 76.447815 76.447815 76.451042 76.380859	25.400034 L1523 31.877089 31.875944 31.849361 31.869553 31.951887 31.850721 31.914982 31.917919 31.941668 31.913567 31.873421 31.808458 31.820160 31.780537 31.807999 31.815182 31.839384 31.760109 31.829580 31.797075 31.766788 31.780506	2.1±0.2 2.2±0.1 7.8±2.0 2.2±0.4 5.7±1.6 2.5±0.3 2.7±0.5 2.3±0.2 2.4±0.4 2.3±0.7 3.3±0.4 1.5±0.4 2.3±0.5 3.0±0.5 3.8±0.9 1.3±0.2 2.5±0.3 2.1±0.6 2.1±0.5 1.7±0.1	57±6 55±8 117±2 147±1 116±8 139±5 122±9 153±3 157±5 136±2 125±6 149±9 154±3 139±8 133±7 127±2 132±7 140±4 133±6 147±4 136±3 142±7 129±7 139±2
76 77 78 79 80 81 82 83 84 85 86 87 88 89 90 91 92 93 94 95 96 97 98 99 100 101	76.134743 75.914574 75.875015 75.943802 75.876350 75.877235 75.949387 75.891914 75.943237 75.877106 75.942673 75.980614 75.935455 75.891846 75.961937 75.912445 75.79404 75.773496 75.774246 75.774246 75.779404 75.773396 75.768265 75.810715 75.808716 75.734344 75.733310 75.778854	25.309156 25.233492 25.201035 25.230867 25.193361 25.189051 25.220924 25.187262 25.202789 25.151016 25.182020 25.184624 25.154423 25.129160 25.160721 25.127752 25.139061 25.314596 25.304075 25.280252 25.294556 25.317068 25.302570 25.261499 25.287922 25.285486	4.4±1.2 9.4±1.0 6.2±1.2 6.1±0.8 3.7±1.0 3.1±0.5 5.4±0.4 2.8±0.5 5.4±0.5 2.8±0.4 4.3±0.6 3.7±0.4 3.7±0.7 3.6±0.8 2.9±0.3 2.8±0.6 2.8±0.3 2.1±0.4 2.4±0.6 3.1±0.6 3.3±0.2 1.8±0.2 2.1±0.5 3.1±0.7	74±8 61±3 80±5 67±3 61±8 67±5 63±2 66±5 61±3 64±3 67±5 73±6 60±8 61±8 61±3 66±6 78±3 78±6 86±7 72±5 66±2 74±3 73±7 78±6		136 1 2 3 4 5 6 7 8 9 10 11 12 13 14 15 16 17 18 19 20 21 22 23	75.998466 76.510254 76.527199 76.524780 76.530388 76.554489 76.537842 76.568336 76.569550 76.595695 76.616318 76.31382 76.362289 76.390350 76.405693 76.405693 76.430855 76.418915 76.455315 76.447815 76.451042 76.380859 76.390282	25.400034 L1523 31.877089 31.875944 31.849361 31.869553 31.951887 31.850721 31.914982 31.917919 31.941668 31.913567 31.873421 31.808458 31.820160 31.780537 31.807999 31.815182 31.839384 31.760109 31.829580 31.797075 31.766788 31.780506 31.808069	2.1±0.2 2.2±0.1 7.8±2.0 2.2±0.4 5.7±1.6 2.5±0.3 2.7±0.5 2.3±0.2 2.4±0.4 2.3±0.7 3.3±0.4 1.5±0.4 2.3±0.5 3.0±0.5 3.0±0.5 3.8±0.9 1.3±0.2 2.5±0.3 2.1±0.6 2.1±0.5 1.7±0.1 2.3±0.3	57±6 55±8 117±2 147±1 116±8 139±5 122±9 153±3 157±5 136±2 125±6 149±9 154±3 139±8 133±7 127±2 132±7 140±4 136±3 147±4 136±3 142±7 129±7 139±2 131±3
76 77 78 79 80 81 82 83 84 85 86 87 88 89 90 91 92 93 94 95 96 97 98 99 100 101 102	76.134743 75.914574 75.875015 75.943802 75.876350 75.877235 75.949387 75.891914 75.942673 75.942673 75.980614 75.935455 75.891846 75.961937 75.912445 75.940964 75.774246 75.774246 75.77826 75.768265 75.810715 75.808716 75.734344 75.778854 75.778854 75.778854 75.754028	25.309156 25.233492 25.201035 25.230867 25.193361 25.189051 25.220924 25.187262 25.202789 25.151016 25.182020 25.184624 25.154423 25.129160 25.160721 25.127752 25.139061 25.314596 25.304075 25.280252 25.294556 25.317068 25.302570 25.287922 25.285486 25.261330	4.4±1.2 9.4±1.0 6.2±1.2 6.1±0.8 3.7±1.0 3.1±0.5 5.4±0.4 2.8±0.5 5.4±0.5 2.8±0.4 4.3±0.6 3.7±0.4 3.7±0.7 3.6±0.8 2.9±0.3 2.8±0.3 2.1±0.4 2.4±0.6 3.1±0.6 3.1±0.6 3.1±0.7 2.4±0.2 2.1±0.5 3.1±0.7 2.4±0.2	74±8 61±3 80±5 67±3 61±8 67±5 63±2 66±5 61±3 64±3 67±5 73±6 60±8 61±8 61±3 66±6 78±3 78±6 86±7 72±5 66±2 74±3 73±7 78±6 76±2		136 1 2 3 4 5 6 7 8 9 10 11 12 13 14 15 16 17 18 19 20 21 22 23 24	75.998466 76.510254 76.527199 76.524780 76.530388 76.554489 76.537842 76.568336 76.569550 76.595695 76.616318 76.611382 76.362289 76.369514 76.380829 76.390350 76.405693 76.405693 76.438855 76.418915 76.455315 76.447815 76.451042 76.380859 76.390282 76.390282 76.393456	25.400034 L1523 31.877089 31.875944 31.849361 31.869553 31.951887 31.850721 31.914982 31.917919 31.941668 31.913567 31.873421 31.808458 31.820160 31.780537 31.807999 31.815182 31.839384 31.760109 31.829580 31.797075 31.766788 31.780506 31.808069 31.805899	2.1±0.2 2.2±0.1 7.8±2.0 2.2±0.4 5.7±1.6 2.5±0.3 2.7±0.5 2.3±0.2 2.4±0.4 2.3±0.7 3.3±0.4 1.5±0.4 2.3±0.5 3.0±0.5 3.8±0.9 1.3±0.2 2.5±0.3 2.1±0.6 2.1±0.5 1.7±0.1 2.3±0.3	57±6 55±8 117±2 147±1 116±8 139±5 122±9 153±3 157±5 136±2 125±6 149±9 154±3 139±8 133±7 127±2 132±7 140±4 136±3 147±4 136±3 142±7 129±7 139±2 131±3 148±6
76 77 78 79 80 81 82 83 84 85 86 87 88 89 90 91 92 93 94 95 96 97 98 99 100 101 102 103	76.134743 75.914574 75.875015 75.943802 75.876350 75.877235 75.949387 75.891914 75.942673 75.942673 75.980614 75.935455 75.891846 75.961937 75.912445 75.940964 75.774246 75.774246 75.774246 75.77836 75.808716 75.78310 75.78310 75.778854 75.754028 75.822212	25.309156 25.233492 25.201035 25.230867 25.193361 25.189051 25.220924 25.187262 25.202789 25.151016 25.182020 25.184624 25.154423 25.129160 25.160721 25.127752 25.139061 25.314596 25.304075 25.280252 25.294556 25.317068 25.302570 25.287922 25.285486 25.261330 25.296404	4.4±1.2 9.4±1.0 6.2±1.2 6.1±0.8 3.7±1.0 3.1±0.5 5.4±0.4 2.8±0.5 5.4±0.5 2.8±0.4 4.3±0.6 3.7±0.4 3.7±0.7 3.6±0.8 2.9±0.3 2.8±0.6 2.8±0.3 2.1±0.4 2.4±0.6 3.1±0.6 3.1±0.6 3.1±0.7 2.4±0.2 2.1±0.5 3.1±0.7 2.4±0.2 2.8±0.6	74±8 61±3 80±5 67±3 61±8 67±5 63±2 66±5 61±3 64±3 67±5 73±6 60±8 61±8 61±3 66±6 78±3 78±6 86±7 72±5 66±2 74±3 73±7 78±6 76±2 85±6		136 1 2 3 4 5 6 7 8 9 10 11 12 13 14 15 16 17 18 19 20 21 22 23 24 25	75.998466 76.510254 76.527199 76.524780 76.530388 76.554489 76.537842 76.568336 76.569550 76.595695 76.616318 76.362289 76.369514 76.380829 76.390350 76.405693 76.405693 76.447815 76.447815 76.447815 76.451042 76.380859 76.390282 76.393456 76.402557	25.400034 L1523 31.877089 31.875944 31.849361 31.869553 31.951887 31.850721 31.914982 31.917919 31.941668 31.913567 31.873421 31.808458 31.820160 31.780537 31.807999 31.815182 31.839384 31.760109 31.829580 31.797075 31.766788 31.780506 31.808069 31.805899 31.822380	2.1±0.2 2.2±0.1 7.8±2.0 2.2±0.4 5.7±1.6 2.5±0.3 2.7±0.5 2.3±0.2 2.4±0.4 2.3±0.7 3.3±0.4 1.5±0.4 2.3±0.5 3.0±0.5 3.8±0.9 1.3±0.2 2.5±0.3 2.1±0.6 2.1±0.5 1.7±0.1 2.3±0.3 2.3±0.3	57±6 55±8 117±2 147±1 116±8 139±5 122±9 153±3 157±5 136±2 125±6 149±9 154±3 139±8 133±7 127±2 132±7 140±4 136±3 142±7 129±7 139±2 131±3 148±6 135±7
76 77 78 79 80 81 82 83 84 85 86 87 88 89 90 91 92 93 94 95 96 97 98 99 100 101 102	76.134743 75.914574 75.875015 75.943802 75.876350 75.877235 75.949387 75.891914 75.942673 75.942673 75.980614 75.935455 75.891846 75.961937 75.912445 75.940964 75.774246 75.774246 75.77826 75.768265 75.810715 75.808716 75.734344 75.778854 75.778854 75.778854 75.754028	25.309156 25.233492 25.201035 25.230867 25.193361 25.189051 25.220924 25.187262 25.202789 25.151016 25.182020 25.184624 25.154423 25.129160 25.160721 25.127752 25.139061 25.314596 25.304075 25.280252 25.294556 25.317068 25.302570 25.287922 25.285486 25.261330	4.4±1.2 9.4±1.0 6.2±1.2 6.1±0.8 3.7±1.0 3.1±0.5 5.4±0.4 2.8±0.5 5.4±0.5 2.8±0.4 4.3±0.6 3.7±0.4 3.7±0.7 3.6±0.8 2.9±0.3 2.8±0.3 2.1±0.4 2.4±0.6 3.1±0.6 3.1±0.6 3.1±0.7 2.4±0.2 2.1±0.5 3.1±0.7 2.4±0.2	74±8 61±3 80±5 67±3 61±8 67±5 63±2 66±5 61±3 64±3 67±5 73±6 60±8 61±8 61±3 66±6 78±3 78±6 86±7 72±5 66±2 74±3 73±7 78±6 76±2		136 1 2 3 4 5 6 7 8 9 10 11 12 13 14 15 16 17 18 19 20 21 22 23 24	75.998466 76.510254 76.527199 76.524780 76.530388 76.554489 76.537842 76.568336 76.569550 76.595695 76.616318 76.611382 76.362289 76.369514 76.380829 76.390350 76.405693 76.405693 76.438855 76.418915 76.455315 76.447815 76.451042 76.380859 76.390282 76.390282 76.393456	25.400034 L1523 31.877089 31.875944 31.849361 31.869553 31.951887 31.850721 31.914982 31.917919 31.941668 31.913567 31.873421 31.808458 31.820160 31.780537 31.807999 31.815182 31.839384 31.760109 31.829580 31.797075 31.766788 31.780506 31.808069 31.805899	2.1±0.2 2.2±0.1 7.8±2.0 2.2±0.4 5.7±1.6 2.5±0.3 2.7±0.5 2.3±0.2 2.4±0.4 2.3±0.7 3.3±0.4 1.5±0.4 2.3±0.5 3.0±0.5 3.8±0.9 1.3±0.2 2.5±0.3 2.1±0.6 2.1±0.5 1.7±0.1 2.3±0.3	57±6 55±8 117±2 147±1 116±8 139±5 122±9 153±3 157±5 136±2 125±6 149±9 154±3 139±8 133±7 127±2 132±7 140±4 136±3 147±4 136±3 142±7 129±7 139±2 131±3 148±6

28	76.412407	31.800669	2.7 ± 0.8	132±8
29	76.424736	31.842855	1.8 ± 0.4	145 ± 7
30	76.412186	31.750330	1.9 ± 0.2	136±2
31	76.418869	31.760103	1.6 ± 0.2	148±4
32	76.436714	31.760065	2.2 ± 0.6	138±7
33	76.455429	31.829636	2.5 ± 0.2	132 ± 2
34	76.447945	31.797152	2.7 ± 0.4	138±4
35	76.456650	31.825886	2.8 ± 0.7	136±7
36	76.451050	31.766825	2.6 ± 0.3	139±3
37	76.464554	31.788027	2.6 ± 0.8	138±8
38	76.480766	31.805689	2.1 ± 0.6	141±8
39	76.487595	31.802568	2.4 ± 0.8	150±9
40	76.496735	31.810266	6.2 ± 0.8	118±4
41	76.488060	31.760403	3.1 ± 0.9	137±8
42	76.501633	31.798565	3.0 ± 0.3	126±3
43	76.390701	31.686728	3.8 ± 0.8	139±6
44	76.398857	31.653662	5.8 ± 1.5	139±7
45	76.411369	31.654001	4.1 ± 0.8	110±6
46	76.404976	31.621721	2.8 ± 0.8	117±8
47	76.421494	31.635687	2.9 ± 0.2	126±2
48	76.444016	31.724058	7.1±1.1	114±5
49	76.454140	31.723234	1.6±0.2	149±3
50	76.455963	31.657572	3.7 ± 0.6	120±5
51	76.449776	31.624134	2.6±0.8	121±9
52	76.455399	31.634275	2.4±0.5	122±6
53	76.460320	31.644791	3.7 ± 0.7	117±5
54	76.478333	31.715322	2.7 ± 0.4	108±4
55	76.468285	31.625584	2.8±0.6	109±6
56	76.477325	31.646517	2.5 ± 0.2	113±2
57	76.477043	31.636938	3.0 ± 0.7	112±6
58	76.500839	31.644615	4.1±0.3	111±2
59	76.511322	31.647291	4.6±1.4	116±9
60	76.532593	31.559700	2.3±0.1	128±1
61	76.556007	31.602110	0.9 ± 0.1	85±3
62	76.548889	31.557184	1.8±0.4	122±6
63	76.558014	31.576170	1.8±0.4	111±7
64	76.575455	31.579693	0.7 ± 0.1	47±5
65	76.590271	31.581350	2.6±0.6	114±6
66	76.587685	31.548935	3.5±0.9	111±8
67	76.607468	31.630785	3.5 ± 0.7	109±5
68	76.600143	31.599745	2.7 ± 0.7	124±7
69	76.620087	31.604908	2.5±0.4	119±4
70	76.626434	31.599918	3.6 ± 0.6	120±4
71	76.626961	31.547365	1.6 ± 0.3	113±6
72	76.628983	31.551390	0.8 ± 0.2	126±6
73	76.650894	31.584427	5.2 ± 0.6	140±3
74	76.669754	31.709686	1.9 ± 0.5	165±7
75	76.682365	31.722557	2.9 ± 0.6	146±6
76	76.683945	31.689857	1.9 ± 0.4	129±5
77	76.682846	31.644882	1.4±0.3	129±6
78	76.704788	31.726807	1.9 ± 0.2	145±3
79	76.709641	31.702108	5.6±0.7	127±4
80	76.706017	31.676428	1.1±0.1	120±3
81	76.700264	31.641378	2.8±0.3	120±3
82	76.728493	31.707870	1.5±0.2	138±4
83	76.730232	31.709875	1.0 ± 0.3	148±7
84	76.728996	31.705322	2.8±0.7	131±7
85	76.728569	31.679085	1.1±0.2	49±5
86	76.735046	31.652258	2.6±0.4	118±5
87	76.736504	31.654655	2.4±0.7	107±8

88	76.732307	31.633623	3.1 ± 0.8	123±7
89	76.752197	31.698269	2.5 ± 0.3	124±4
90	76.745583	31.664951	2.9 ± 0.8	114±8
91	76.756363	31.706753	2.3 ± 0.3	132 ± 4
92	76.759010	31.713301	1.5 ± 0.3	130±6
93	76.768112	31.700790	2.1 ± 0.5	138 ± 7
94	76.761971	31.670368	2.2 ± 0.6	106 ± 8
95	76.760277	31.646980	1.2 ± 0.2	126±4
96	76.781097	31.678493	0.5 ± 0.1	53±6
97	76.776329	31.647587	1.5 ± 0.4	124±6

This paper has been typeset from a $T_EX/I_E^2T_EX$ file prepared by the author.